Cai *et al. Chem Synth* 2024;4:54
DOI: 10.20517/cs.2024.15

Chemical Synthesis

Review

Open Access

Check for updates

Recent progress in electrochemical synthesis of urea through C-N coupling reactions

Haoxiang Cai[1], Junyang Ding[1,*], Tong Hou[1], Tianran Wei[1], Qian Liu[2], Jun Luo[3], Ligang Feng[4], Wenxian Liu[5,*], Xijun Liu[1,*]

[1]State Key Laboratory of Featured Metal Materials and Life-cycle Safety for Composite Structures, Guangxi Key Laboratory of Electrochemical Energy Materials, MOE Key Laboratory of New Processing Technology for Nonferrous Metals and Materials, School of Resources, Environment and Materials, Guangxi University, Nanning 530004, Guangxi, China.
[2]Institute for Advanced Study, Chengdu University, Chengdu 610106, Sichuan, China.
[3]ShenSi Lab, Shenzhen Institute for Advanced Study, University of Electronic Science and Technology of China, Shenzhen 518110, Guangdong, China.
[4]School of Chemistry and Chemical Engineering, Yangzhou University, Yangzhou 225002, Jiangsu, China.
[5]College of Materials Science and Engineering, Zhejiang University of Technology, Hangzhou 310014, Zhejiang, China.

[*]**Correspondence to:** Dr. Junyang Ding, Dr. Xijun Liu, State Key Laboratory of Featured Metal Materials and Life-cycle Safety for Composite Structures, Guangxi Key Laboratory of Electrochemical Energy Materials, MOE Key Laboratory of New Processing Technology for Nonferrous Metals and Materials, School of Resources, Environment and Materials, Guangxi University, No.100, East Daxue Road, Xixiangtang District, Nanning 530004, Guangxi, China. E-mail: junyangding@stud.tjut.edu.cn; xjliu@gxu.edu.cn; Dr. Wenxian Liu, College of Materials Science and Engineering, Zhejiang University of Technology, No. 18, Chaowang Road, Dushu District, Hangzhou 310014, Zhejiang, China. E-mail: liuwx@zjut.edu.cn

How to cite this article: Cai H, Ding J, Hou T, Wei T, Liu Q, Luo J, Feng L, Liu W, Liu X. Recent progress in electrochemical synthesis of urea through C-N coupling reactions. *Chem Synth* 2024;4:54. https://dx.doi.org/10.20517/cs.2024.15

Received: 31 Jan 2024 **First Decision:** 13 Jun 2024 **Revised:** 13 Jul 2024 **Accepted:** 27 Aug 2024 **Published:** 6 Sep 2024

Academic Editor: Xiangdong Yao **Copy Editor:** Pei-Yun Wang **Production Editor:** Pei-Yun Wang

Abstract

The traditional industry synthesizes urea through the reaction of NH_3 and CO_2 under high temperatures and pressure. Electrochemical catalysis, which could replace the traditional ammonia synthesis route, i.e., co-reduces carbon dioxide with nitrogen sources [nitrite (NO_2^-), nitrate (NO_3^-), nitrogen (N_2), and nitric oxide (NO)] to synthesize urea, is a promising strategy for the synthesize of urea under environmental conditions. Unlike traditional industry routes, electrochemical catalysis urea synthesis is beneficial for both resource utilization and environmental protection. Herein, the recent research progress of electrocatalytic urea synthesis is summarized, with emphasis on the design and preparation of the catalyst for the coupling of CO_2 and nitrogen species directly to urea. The involved reaction mechanism of C-N coupling is generalized and discussed. Furthermore, the difficulties and challenges at the present stage are summarized, and the development direction of electrocatalytic synthesis of urea is prospected.

Keywords: Urea electrosynthesis, C-N coupling reaction mechanism, metallic catalyst, metal compound catalyst

INTRODUCTION

The fast growth of the world economy, especially the chemical industry, relies heavily on fossil fuels, resulting in the rapid consumption of these non-renewable resources[1]. Meanwhile, large quantities of CO_2 gas generated by fuel combustion are emitted into the atmosphere, further leading to the global greenhouse effect and ocean acidification[2]. Furthermore, as a result of the impact of human activities, such as industrial waste emissions and overfertilization[3], sewage containing high concentrations of active nitrogen pollutants [such as nitrite (NO_2^-) and nitrate (NO_3^-)] is discharged and accumulated, leads to the pollution of underground water sources, which makes human health and the biological environment be at risk[4]. Therefore, the conversion of CO_2 and nitrogen pollutants into chemical products with high added value is an economically viable strategy that can guarantee the sustainability of energy, and alleviate environmental problems.

Urea [$CO(NH_2)_2$], as the first organic compound synthesized from inorganic feedstock, is one of the most profitable industrial products among CO_2 derivatives[5]. The high nitrogen content of 46% makes urea the well-known nitrogenous fertilizer, accounting for 70% of the world's nitrogen fertilizer, feeding 19% of the global population so far. Besides being a fertilizer, urea is also widely used in other chemical applications. For instance, in the production of melamine and urea-formaldehyde resins, it is the raw material[6]. In the pharmaceutical field, urea is the starting material for the production of barbiturates central nervous system depressants[7]. Moreover, its consumption is growing at an annual rate of more than 3%.

Nevertheless, the traditional industrial urea synthesis process involves the reaction of carbon dioxide and liquid ammonia under extreme conditions of high pressures (150~250 bar) and temperatures (150~210 °C)[8], complex equipment in a centralized chemical plant, and multi-cycle processes to improve catalytic efficiency[9]. In addition, the production of urea needs about 80% of the ammonia produced worldwide[10], of which is mainly obtained by artificial nitrogen-fixing that uses N_2 and H_2 as feedstocks in the Haber-Bosch process[11]. And it is also an energy-intensive reaction that consumes 2% of global energy due to the N≡N triple bond with a high bond energy of 940.95 kJ·mol^{-1}[12]. In brief, the harsh reaction process and large energy expenditure are huge obstacles to the sustainable strategy for urea manufacture[13].

In comparison to the energy-intensive process of industrially urea synthesis, electrocatalysis is a technically feasible zero-carbon-emission pathway for obtaining value-added products under environmental conditions[14]. And the conversion of CO_2 and reactive nitrogen species into urea molecules through a sustainable production process is of great importance for the development of human society and the reduction of environmental stress[15,16]. The electrocatalytic urea synthesis includes the reduction reaction of CO_2 (CO_2RR), the reduction reaction of nitrogen-based species (NRR), and the competitive hydrogen evolution reaction (HER), the latter of which results in increased by-products and reduced urea yield[17]. What is more, the key C-N coupling step in the electrosynthesis of urea consumingly depends on the surface electronic state and chemical composition of the catalyst. Thus, for the purpose of pursuing the efficient manufacture of urea, the following factors should be considered when designing the electrocatalysts, i.e., not only to meet the coactivation reaction of the raw materials but also to consider the reaction of the intermediates, so as to build efficient active sites conducive to C-N coupling.

Considering the great progress, it is important to review the relevant works on electrocatalytic urea synthesis. Recently, Jiang *et al.* have summarized recent advances in electrocatalytic urea synthesis with emphasis on C-N coupling reaction mechanisms by classifying N sources[18]. Nevertheless, a timely review paper highlighting preparation methods and structure-activity relationships of advanced catalysts for urea

synthesis through C-N coupling reactions is needed. Herein, the reaction pathways and C-N coupling mechanisms of urea electrocatalytic synthesis are summarized in detail. Different from the previous review papers, we categorize the catalysts in terms of different material systems. This categorization is beneficial for evaluating the advantages and disadvantages of the materials belonging to the same system and guiding the design and optimization strategies of catalysts. At the end of the review, we discuss the shortcomings and impediments for electrocatalytic urea synthesis under ambient conditions, providing personal insight for development.

THE MECHANISM OF C-N COUPLING

The key to enhancing the electrocatalytic urea synthesis efficiency is the regulation of the C-N coupling reaction originating from CO_2 and nitrogenous species. The research of the C-N coupling principle, the electronic/coordination structure of active sites, and the determination of intermediates in the urea production process is helpful in the design of efficient catalysts theoretically[19].

NO_2^- as nitrogen sources

In 1995, Shibata *et al.* pioneered the electrochemical synthesis of urea under standard atmosphere and ambient temperature and briefly mentioned the mechanism of urea electrosynthesis[20]. In their opinions, the simultaneous existence of activated CO (i.e., adsorbed CO) and ammonia intermediate was a necessary condition for the electrocatalytic synthesis of urea. They predicted that the active substances could come from CO_2 and simple ammonia compounds such as NO_3^-/NO_2^-, respectively. However, it had been proved by comparative experiments that substituting NH_3 for NO_2^- or CO for CO_2 could not achieve the electrosynthesis of urea. So it could be concluded that urea was produced while NO_2^- and CO_2 were reduced at the same time; i.e., the NO_2^- was reduced to an ammonia intermediate, which further reacted with adsorbed CO.

Up to now, it is not difficult to conclude from previous reports that the mechanism of urea electrosynthesis mostly depends on the conversion of CO_2 to $^*CO$ and the conversion of NO_2^- to $^*NH_2$ at catalytic sites. Especially in urea electrosynthesis with NO_2^- as raw material, it is a general rule that the two important intermediates ($^*CO$ and $^*NH_2$) can form the NH_2CONH_2 structure by C-N coupling [Figure 1A].

As shown in the work of Cao *et al.*, the co-reduction of CO_2 and NO_2^- was realized on Cu-TiO_2 catalysts with oxygen-rich vacancies[21]. The $^*CO$ was produced by electrocatalytic reduction of CO_2 at the low-valence Cu sites; meanwhile, NO_2^- was converted to $^*NH_2$ precursor by a reduction reaction at the active sites of bi-Ti^{3+}. Subsequently, the C-N coupling of the two precursors originates $^*NH_2CONH_2$ species, which desorbed to form urea.

The overall reactions are expressed as follows:

$$CO_2 + 2H^+ + 2e^- \rightarrow CO^* + H_2O \quad (1)$$

$$NO_2^- + 6H^+ + 6e^- \rightarrow NH_2^* + 2H_2O \quad (2)$$

$$CO^* + 2NH_2^* \rightarrow NH_2CONH_2 \quad (3)$$

In order to unravel the reaction mechanism, Feng *et al.* carried out control experiments via CO_2-temperature-programmed desorption (TPD) and electrochemical CO-stripping measurement [Figure 2A-C], and the density functional theory (DFT) theoretical calculation was also implemented[22].

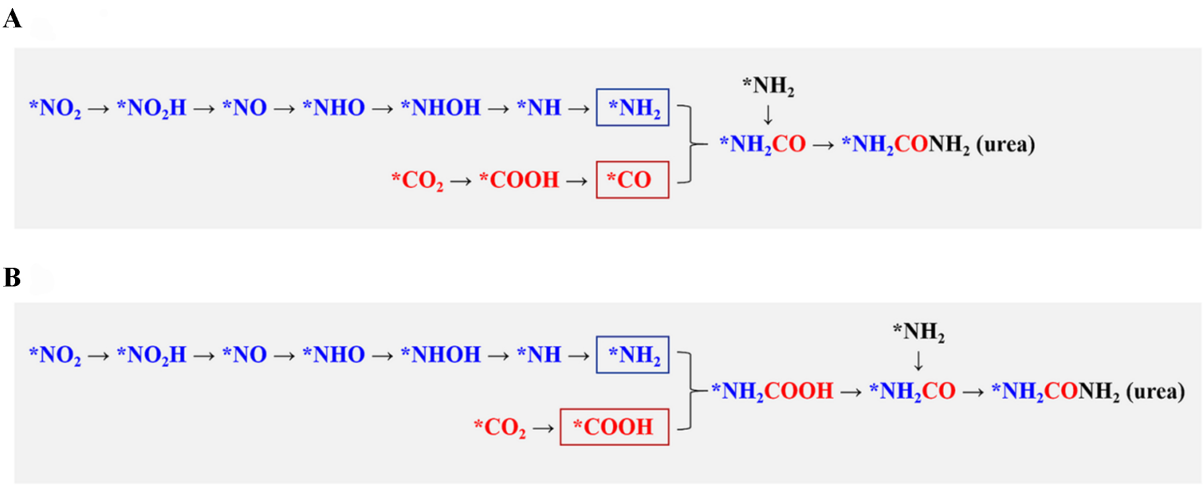

Figure 1. The reaction pathway for the electrosynthesis of urea by co-reduction of NO_2^- and CO_2. (A) The pathway for the C-N coupling of $^*NH_2$ and $^*CO_2$ intermediates; (B) The pathway for the C-N coupling of $^*NH_2$ and $^*COOH$ intermediates.

The results showed that CO_2 and NO_2^- were reduced to $^*CO$ and $^*NH_2$, and coupled to form $^*CONH_2$, which was further converted to urea over the Te-Pd nanocrystals (NCs)/C catalyst [Figure 2D].

It is worth noting that in the oxygen vacancy-rich ZnO system reported by Meng *et al.*, the abundant oxygen vacancies (OVs) significantly reduced the interfacial charge transfer resistance of the catalyst[23,24]. This report used *in situ* attenuated total reflection Flourier transformed infrared (ATR-FTIR) to characterize the reaction process of CO_2 with NO_2^-. As shown in Figure 2E, under the CO_2 alone atmosphere, the signals detected at 1,360 and 1,210 cm^{-1} belonged to $^*COOH$, and its peak increased with decreasing potentials. In the presence of NO_2^- alone, the signals belonging to NH_3 and NO_2^- were detected at 1,100 and 1,220 cm^{-1}, respectively. The NO_2^- signal exhibited a rising peak due to its depletion. In the case of co-catalyzed CO_2 and NO_2^-, the $^*COOH$ signal at 1,210 cm^{-1} was offset by the NO_2^- signal at 1,220 cm^{-1}, and no $^*COOH$ signal peak was observed at 1,360 cm^{-1}, suggesting that $^*COOH$ was consumed during urea synthesis. Moreover, the C–N bond signal was detected at 1,440 cm^{-1}. The ATR-FTIR results could guide the possible reaction pathways: the O atoms in NO_2^- filled the surface OVs, and then formed $^*NH_2$ intermediates through multistep proton-coupled electron transfer (PCET) process [Figure 2E and F]; the CO_2 entered the vacancies was transformed into $^*COOH$ intermediates; urea was synthesized via subsequent coupling of $^*NH_2$ and $^*COOH$ intermediates [Figure 1B][25,26].

NO as nitrogen sources

As mentioned previously, $^*NO$ is a key intermediate for NO_3^-/NO_2^- electroreduction. Therefore, Huang *et al.* proposed a urea production strategy, i.e., direct reduction of NO and CO_2 through the prepared Zn nanobelts (Zn NBs) catalysts[27]. Online differential electrochemical mass spectroscopy (DEMS) measurement was used to detect the intermediates and products in urea synthesis reactions, and the signals attributed to NH_2OH, HNO, NH_3, and CO/N_2 were periodically detected [Figure 3A]. In this case, the signals of NH_3 and N_2 came from the by-products of the reaction process. The ATR-FTIR was also performed to capture the absorbed intermediates [Figure 3B]. When NO and CO_2 were co-reduced, a vibrational band appeared at 1,465 cm^{-1}, which belonged to the C–N bond.

The DFT calculations revealed that NO electrochemical reduction followed the nitrogen-alternating pathway[28]: $^*NO \rightarrow ^*NHO \rightarrow ^*NHOH$ ($^*HNOH$, equally) $\rightarrow ^*NH_2OH \rightarrow ^*NH_2 \rightarrow ^*NH_3$, while CO_2-to-CO

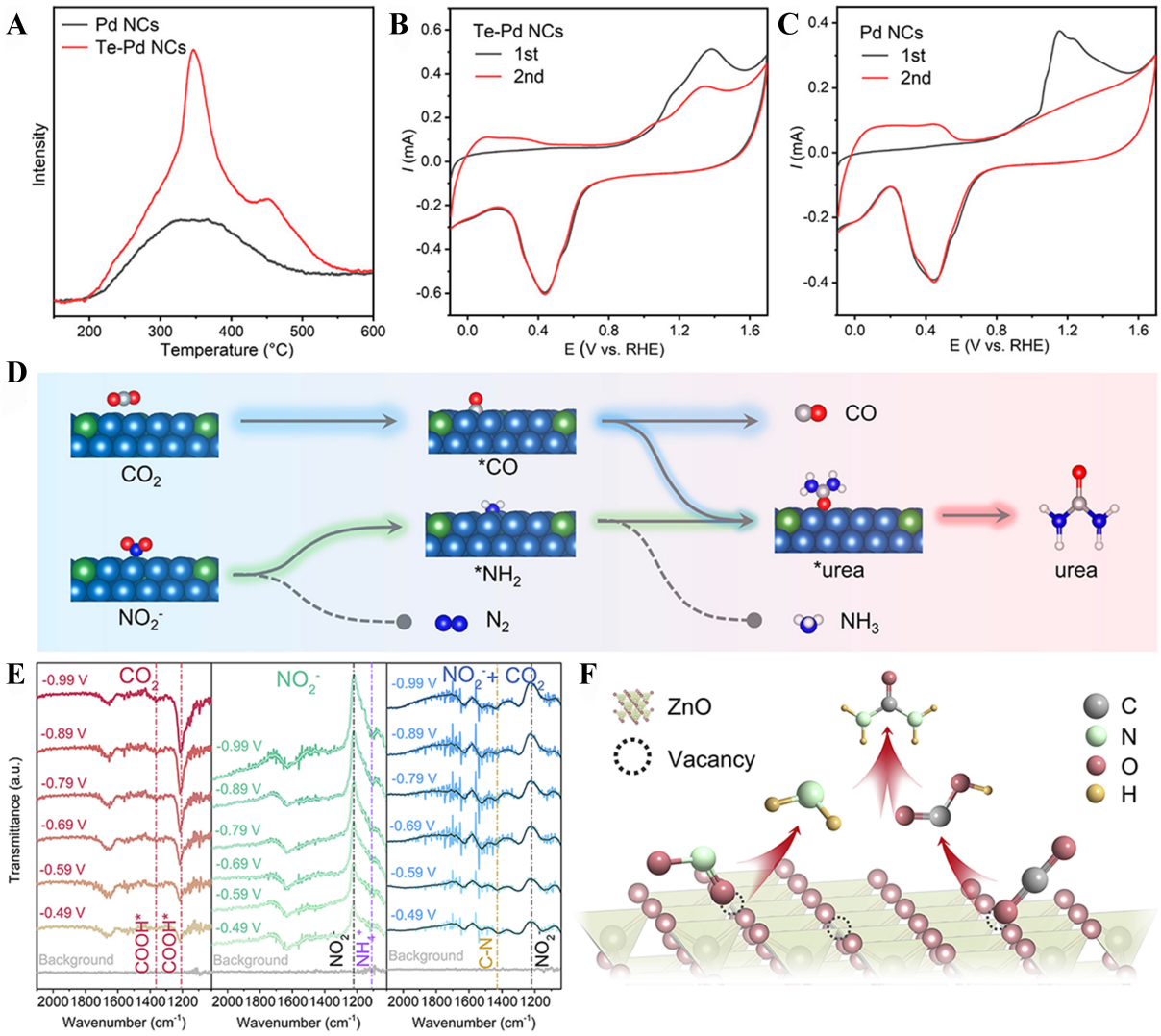

Figure 2. (A) CO_2-TPD for Pd NCs and Te-Pd NCs; CO-stripping measurements for (B) Te-Pd NCs/C and (C) Pd NCs/C (0.1 M $KHCO_3$ solution, the scanning rate is 20 $mV \cdot s^{-1}$, the first cycle has a CO absorbed adlayer and the second cycle does not. Dose CO for 30 min before measuring); (D) Schematic diagram for urea electrosynthesis from CO_2RR and NO_2^-RR at Te-Pd NCs. Reprinted with permission from ref[22]. Copyright 2020 American Chemical Society; (E) *In situ* ATR-FTIR spectra for ZnO-V under CO_2, $NaNO_2$, and both; (F) Schema of urea synthesis on ZnO-V. Reprinted with permission from ref[23]. Copyright 2021 The Authors. Cell Reports Physical Science published by Elsevier. TPD: Temperature-programmed desorption; NCs: nanocrystals; CO_2RR: reduction reaction of CO_2; ATR-FTIR: attenuated total reflection Flourier transformed infrared.

conversion involved *COOH and *CO intermediates. The specific reaction pathway could be explained as follows: in the process of conversion from CO_2 to CO, the existence of absorbed NO was capable of further stabilizing *COOH and *CO intermediates. However, the binding of *COOH to nitrogen-related intermediates (*NO, *NHO, *NHOH, $^*NH_2OH$, and $^*NH_2$) was energy unstable. The energy required to form $^*CO\text{-}NH_2$ was -0.46 eV, and the energy barrier of $^*CONH_2$ formation had a moderate Ea value (+0.85 eV), which was kinetically favorable for the formation of C–N bonds [Figure 3C]. Notably, the desorption of *CO was the potential-determining step (PDS). The second C-N coupling tended to be achieved by the coupling of $^*CONH_2$ and $^*NH_2$ according to theoretical calculations [Figure 3D]. Thus, it was deduced that the urea electrosynthesis reaction pathway for co-reduction of NO and CO_2 was realized via the step coupling of *CO and $^*NH_2$ [Figure 3E].

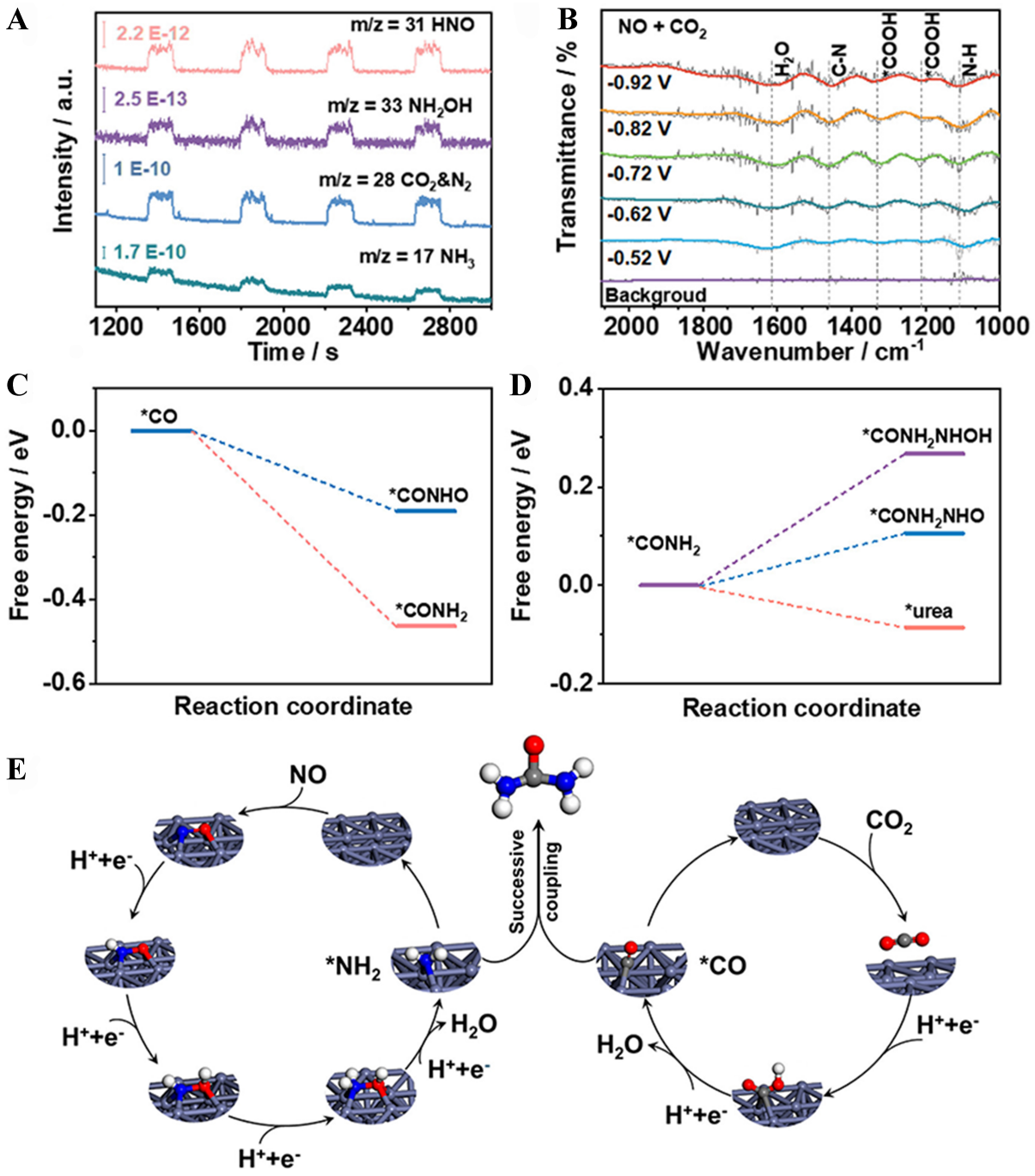

Figure 3. (A) Online DEMS measurements and (B) *In situ* ATR-FTIR spectra on Zn NBs; (C and D) Free energy changes to form (C) The first C–N bond and (D) The second on the surface of Zn(101); (E) Scheme of urea synthesis mechanism on the Zn surface with NO and CO_2 as raw materials. Reprinted with permission from ref[27]. Copyright 2022 American Chemical Society. DEMS: Differential electrochemical mass spectroscopy; ATR-FTIR: attenuated total reflection Flourier transformed infrared; Zn NBs: Zn nanobelts.

NO_3^- as nitrogen sources

Although most studies have shown that the C-N coupling process follows the law of the conversions of CO_2 to $^*CO$ and NO_2^- to $^*NH_2$, compared to NO_2^-, the urea electrochemical synthesis with NO_3^- as the nitrogen source shows obvious distinct mechanisms in different catalytic systems. The reaction pathway for the electrosynthesis of urea by co-reduction of NO_3^- and CO_2 is displayed in Figure 4.

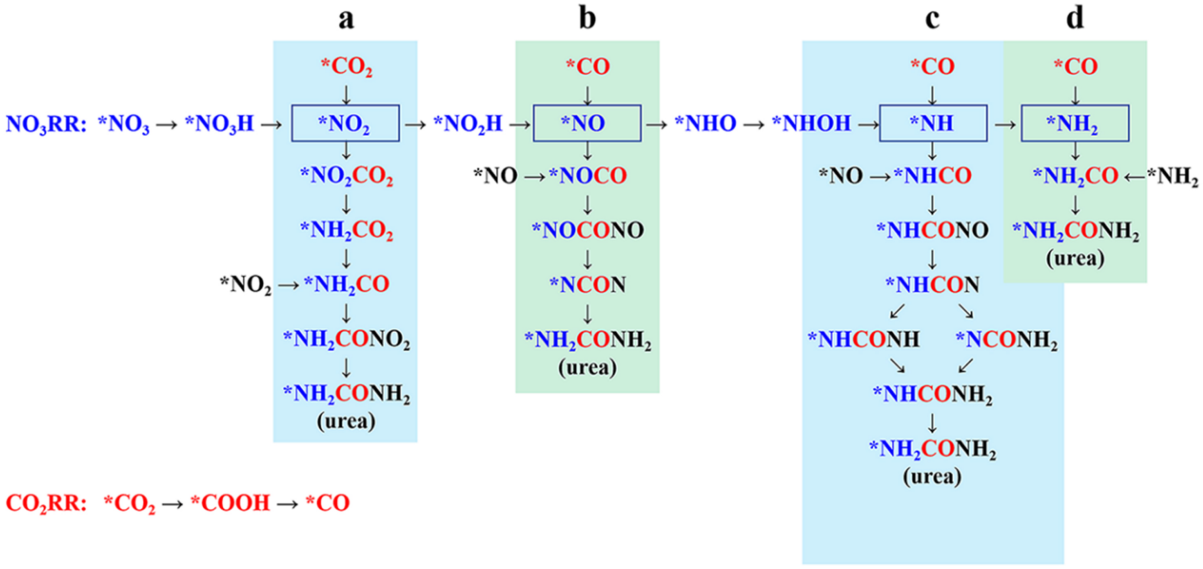

Figure 4. The reaction pathway for the electrosynthesis of urea by co-reduction of NO_3^- and CO_2.

In the experiment reported by Lv *et al.*, on the {100} facets of $In(OH)_3$, the NO_3^- was thermodynamically reduced to $^*NO_2$ intermediates, while the protonation process of CO_2 required an additional 0.38eV of energy[29]. On the two coordinated unsaturated In atoms, the electron was transferred to $^*NO_2$. The local "In-O-C-O-In" configuration supported the transfers of electrons to $^*CO_2$. The reaction between the two intermediates of $^*NO_2$ and $^*CO_2$ achieved an early direct C-N coupling. This conclusion was confirmed by a contrast electrocatalysis test. The lower energy barrier formed by $^*CO_2NO_2$ (0.35 eV) contributed to the selective production of urea compared to that for protonating $^*NO_2$ to $^*HNO_2$ (0.62 eV). Further protonation tended to form $^*CO_2NH_2$ intermediates; the rate-determining step of urea electrosynthesis occurred when $^*CO_2NH_2$ intermediates were protonated to $^*COOHNH_2$, which required an increase in free energy of 1.58 eV. Subsequently, the thermodynamically favorable second step of C-N coupling and urea generation occurred. In another report about the indium oxyhydroxide (InOOH) electrocatalyst with defect engineering created by OVs, the authors used advanced operando synchrotron radiation-Fourier transform infrared spectroscopy (SR-FTIR) to further verify the synthesis mechanism of urea and reached the same conclusion as above [Figure 5A and B][30]. The pathway of catalytic reaction and C-N coupling is shown in Figure 4A. It is noteworthy that the reaction pathway of the Zn/Cu hybrid catalyst reported by Luo *et al.* with excellent Faradaic efficiency (FE) of 75% is also consistent with Figure 4A[31]. They utilized *in situ* surface-enhanced Raman spectroscopy (SERS) to observe the intermediates on the catalyst during urea synthesis. Under the conditions of electrocatalytic urea synthesis, the signals located at 334~337 cm^{-1} belonging to M-$OCONH_2$, i.e., the characteristic signal of $^*CO_2NH_2$ intermediates, were observed in both the electrolyte (1 M $KHCO_3$ + 1 M KNO_3) and the reference solution (ammonium carbamate, NH_2COONH_4), while they were not detected in the $KHCO_3$ solution. It confirmed the presence of $^*CO_2NH_2$ intermediates during the catalytic process. For single-component Cu catalyst (electrolyte: 1 M $KHCO_3$ + 1 M KNO_3), these signals were also not detected, indicating that Zn was crucial for the formation of the $^*CO_2NH_2$ intermediate. The *in situ* infrared reflection-absorption spectroscopy (IRRAS) confirmed the critical step in the process where $^*CO_2NH_2$ protonation to $^*COOHNH_2$ occurred.

For works on the electrocatalytic synthesis of urea reported by other groups, the core-shell structure Cu@Zn catalyst designed by Meng *et al.* was conducive to improving the generation of $^*NH_2$ and $^*CO$ intermediates

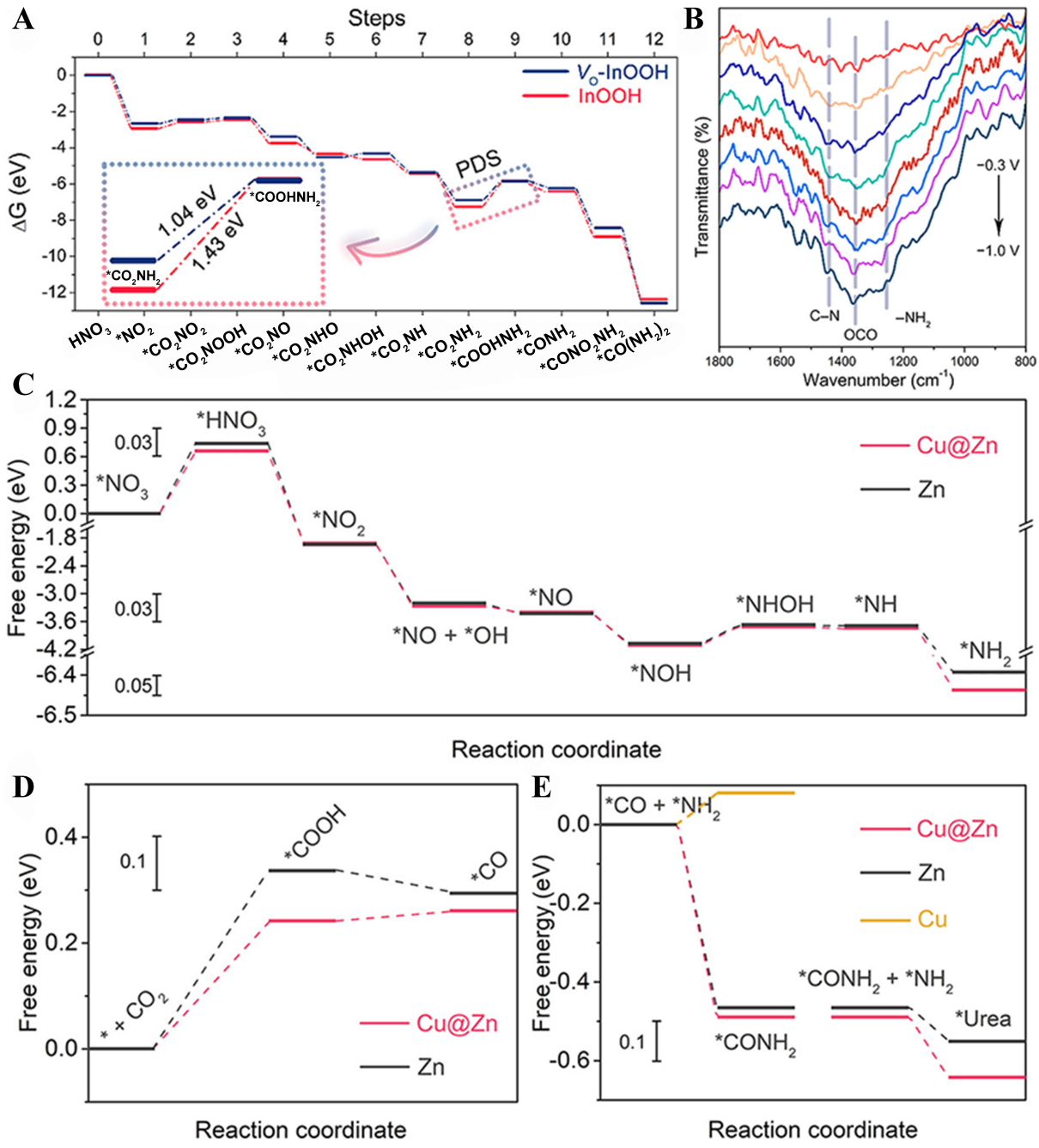

Figure 5. (A) Free energy of urea synthesis on the {010} facets at Vo-InOOH and original InOOH; (B) Infrared signals (800 to 1,800 cm^{-1}) obtained from operando SR-FTIR at potentials of -0.30 to -1.00 V (*vs.* RHE) on Vo-InOOH during the C-N coupling. Reprinted with permission from ref[30]. Copyright 2022 American Chemical Society; (C and D) Free energy of reduction (C) $^*NO_3$ to $^*NH_2$, (D) CO_2 to CO; (E) Free energy of C-N coupling on the surface of Cu@Zn, Zn, and Cu. Reprinted with permission from ref[32]. Copyright 2022 American Chemical Society. InOOH: Indium oxyhydroxide; SR-FTIR: synchrotron radiation-Fourier transform infrared spectroscopy; RHE: reversible hydrogen electrode.

and accelerating the combination of $^*NH_2$ and $^*CO$ to produce urea [Figure 4D][32]. Nevertheless, the DFT results showed that the transition from $^*NO_3$ to $^*HNO_3$ and the formation of $^*COOH$ in the reduction of CO_2 to $^*CO$ were potential limiting steps [Figure 5C-E]. Theoretical calculations by Leverett *et al.* also showed that the formation of $^*COOH$ intermediates at the early stage was the rate-determining step in urea production[33].

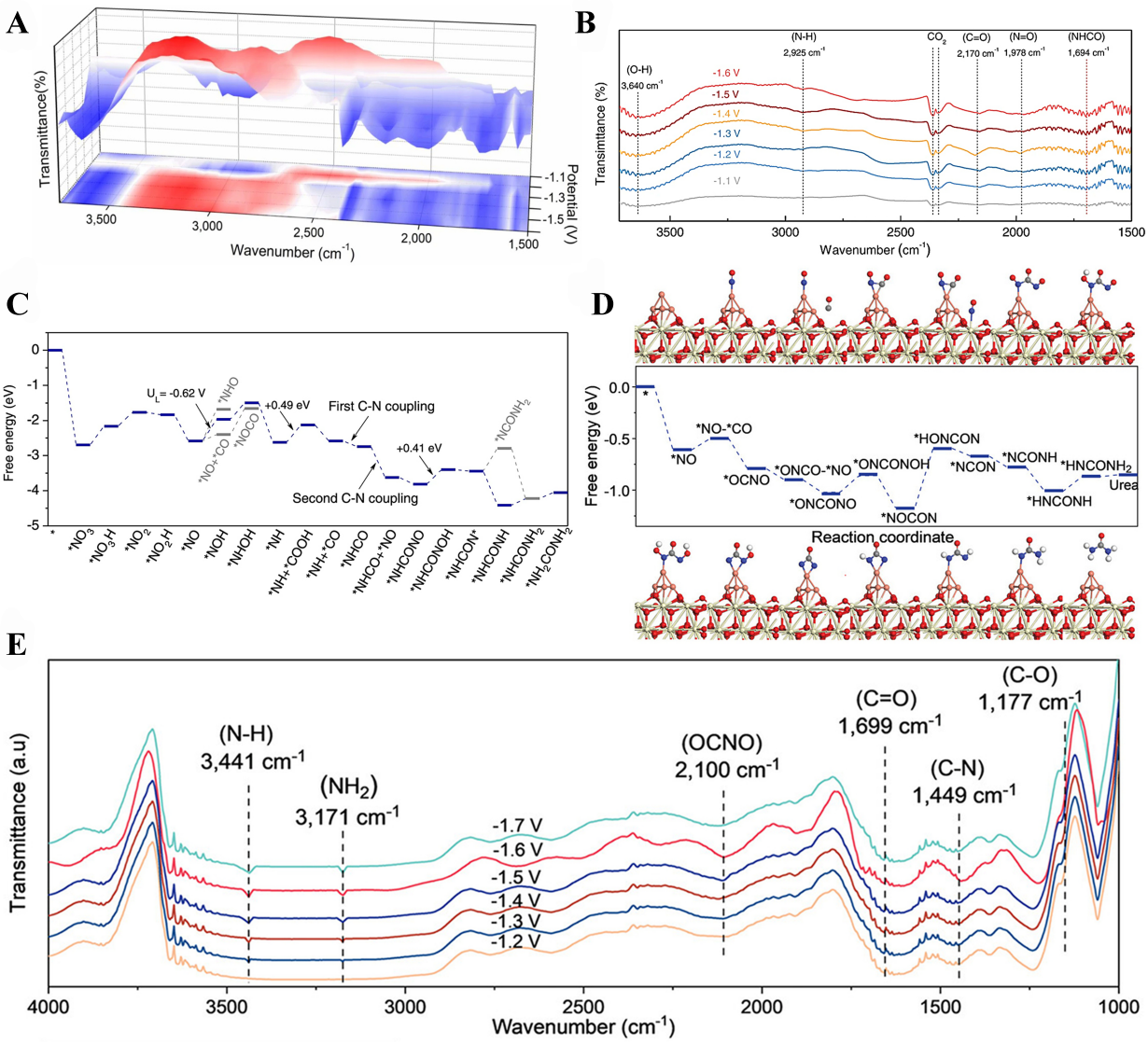

Figure 6. (A) 3D operando SR-FTIR spectra for B-FeNi-DASC; (B) Infrared signal (range 1,500 to 3,750 cm^{-1}) at different potentials for B-FeNi-DASC during C-N coupling; (C) Free energy for B-FeNi-DASC of urea synthesis. Reprinted with permission from ref[34]. Copyright 2022 Nature Publishing Group; (D) Geometric structure and free energy of C-N coupling process at Cu_4-CeO_2 (H, C, N, O, Cu, and Ce atoms are labeled as white, gray, blue, red, pink, and yellow balls in the geometric structure, respectively); (E) Operando SR-FTIR spectroscopy at different potentials for Cu_1-CeO_2 during the C-N coupling. Reprinted with permission from ref[35]. Copyright 2023 Wiley-VCH GmbH. 3D: Three-dimensional; SR-FTIR: synchrotron radiation-Fourier transform infrared spectroscopy; B-FeNi-DASC: bonded Fe-Ni diatomic sites catalyst.

Zhang *et al.* carried out operando SR-FTIR measurement and DFT calculation for bonded Fe-Ni diatomic sites catalyst (B-FeNi-DASC) [Figure 6A-C][34]. The theoretical calculation results showed that the applied potential required for driving the CO formation was +0.32 eV at Fe-Ni bimetallic sites, which is much lower than the free energies for the generation of the key intermediate *COOH for the monometallic atom catalysts (up to +1.88 eV for Fe-N_4 and +2.31 eV for Ni-N_4), and thus, CO_2 was preferentially reduced to *CO intermediate. NO_3^- was reduced to *NO, but the direct coupling of *CO and *NO was disadvantageous in energy (+0.81 eV). So the C-N coupling should follow another path. The *NO intermediate might be

reduced to *NOH or *HNO. The formation of *HNO (+0.62 eV) was more favorable to thermodynamics than that of *NOH (+0.90 eV). Subsequently, *NOH was further dissociated from *NH by two protonations. At the Fe-Ni bonding site, a thermodynamically spontaneous and dynamically feasible coupling occurred between *NH and *CO with a corresponding energy barrier of +0.21 eV, which was further supported by operando SR-FTIR results. The vibration intensity of the infrared bands near 1,694 cm^{-1} increases with the increase of applied negative potential, and reaches its highest value at around -1.50 V, indicating the formation of the intermediate species *NHCO. The next NO would subsequently attach to the Ni site and promptly bind to *NHCO, transforming into the important intermediate *NHCONO, followed by continuous PCET processes that realize the formation of urea [Figure 4C].

In the latest report, Wei *et al.* modified copper monoatoms on the CeO_2 vector (Cu_1-CeO_2) to catalyze the synthesis of urea[35]. DFT calculation results indicated that the *OCNO intermediate was formed by the Eley-Raideal (ER) mechanism. For the purpose of synthesizing urea, a second *NO needs to be introduced into the system to combine with *OCNO [Figure 4B]. The *ONCONO was formed exothermic and subsequently reduced to urea by eight electron-proton-transfer steps. The forming of *HONCONO was the potential limiting step that required free energy of +0.58 eV [Figure 6D]. The cutting-edge operando SR-FTIR measurements and controlled electrolysis experiments showed that urea was formed from key intermediates *OCNO [Figure 6E].

N_2 as nitrogen sources

It is noted that in the case of complex catalyst systems, the C-N coupling process with N_2 as nitrogen sources reaches agreement on key intermediates, focusing on the formation of intermediate *NCON. Subsequent hydrogenation processes may have two reaction pathways, depending on the alternative and distal mechanisms[Figure 7].

On the surface of the $Ni_3(BO_3)_2$ electrocatalyst with Lewis pairs [frustrated Lewis pairs (FLPs)] designed by Yuan *et al.*, the involved hydroxyl, and adjacent Ni sites served as Lewis base (LB) and acid (LA), respectively[36]. FLPs could achieve efficient adsorption of N_2 and CO_2 by unique orbital interaction[37]. The occupied π orbitals of CO_2 contributed electrons to the d empty orbitals on the LA sites while the σ^* empty orbitals of CO_2 received electrons from the LB centers, thereby achieving the activation of CO_2. The interaction between occupied σ orbital on N_2 and the d empty orbital on the LA Ni sites would weaken the N≡N bond, in other words, depleting a large number of electrons in the σ state of N_2 [Figure 8A]. The "donation-acceptance" course at the FLP sites would effectually polarize the reactant molecules, stretching the chemical bond until it eventually broke[38]. Subsequently, through "σ orbital electron transfer", the spontaneous C-N coupling of the *CO with *N=N* intermediates generated the *NCON* intermediate. The conversion of *NCON* intermediate to *NCONH required a free energy of 0.76 eV, which was considered the PDS of the whole reaction. Yuan *et al.* used the Mott-Schottky Bi-$BiVO_4$ heterostructure in another experiment[39]. First, spontaneous charge transferred at the interface of the heterogeneous structure promoted the formation of a space charge region in which N_2/CO_2 was directionally adsorbed via electrostatic interaction[40]. Then, the *CO and *N=N* formed the *NCON* intermediate by electrocatalytic C-N coupling reactions [Figure 8B and C]. Subsequently, the hydrogenation process was more inclined to follow the alternative mechanism to produce urea.

The research of Chen *et al.* supported the same opinions[13]. The DFT results indicated that the side-on configuration on the PdCu surface favors the feedback of electrons from the d orbitals of Pd and Cu into the π^* orbitals of N_2, lowering the order of the N–N bond. The *N=N* directly coupled with CO formed the urea precursor *NCON*, and this process was thermodynamically and kinetically feasible. In the subsequent

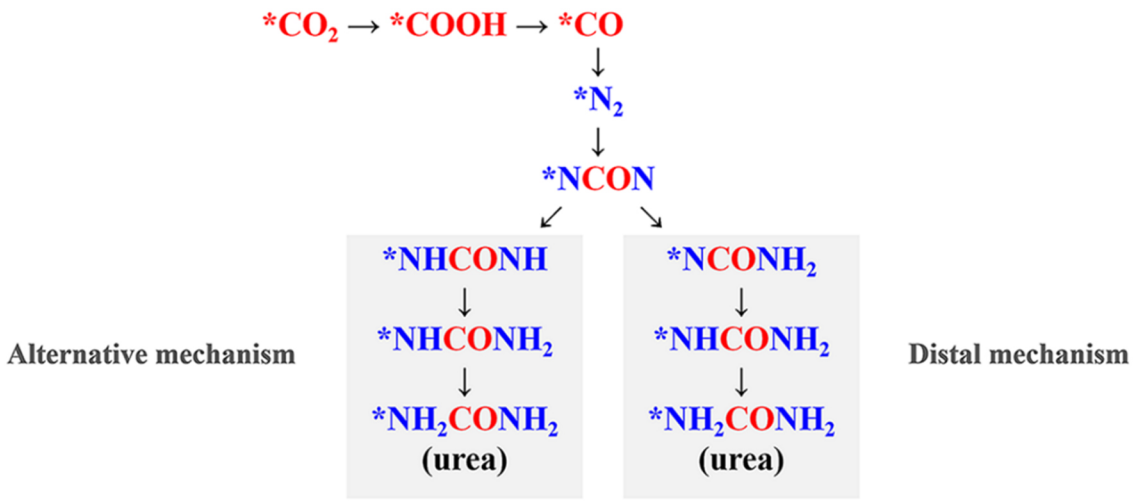

Figure 7. The reaction pathway for the electrosynthesis of urea by co-reduction of N_2 and CO_2.

hydrogenation step, the *NCON* formed the *NCONH structures. The second protonic step might have two reaction pathways, *NCONH$_2$ and *NHCONH, depending on the distal and alternating mechanisms[41]. The third proton-coupling process was the potential limiting step in urea production, requiring +0.64 and +0.78 eV energies for the distal and alternative mechanisms, respectively [Figure 8D].

Above all, the reaction pathways for urea synthesis using NO_2^- or NO as nitrogen sources mostly prefer the C-N coupling of $^*NH_2$ and *CO intermediates, except for the ZnO-Vo catalyst reported by Meng *et al.*, which followed the coupling of $^*NH_2$ and *COOH intermediates[23]. This universal phenomenon can be attributed to the unstable binding of *COOH to N-related intermediates (e.g., *NO, *NHO, *NHOH, $^*NH_2OH$, and $^*NH_2$), while *COOH → *CO is usually a thermodynamically spontaneous process. Compared to other N sources, the pathways that use NO_3^- as N sources have different positions for the C-N coupling in various catalysts. The possible reason for this phenomenon is that the reduction reaction of NO_3^- (NO_3^-RR) has the largest number of protonation steps, which provides a rich variety of N-related intermediates. In this case, several intermediates (e.g., $^*NO_2$, *NO, *NH, and $^*NH_2$, as shown in Figure 4) have the potential to serve as key intermediates for C-N coupling. For the system that uses N_2 as a nitrogen source, the electrocatalytic C-N coupling processes are all realized by the insertion of *CO onto $^*N_2$ after the elongation of the N≡N bond. The initial coupling of *CO to $^*N_2$ will benefit from the matching of the molecular orbital symmetry of the two intermediates. Subsequent hydrogenation will follow either the alternative or distal mechanism [Figure 7]. It depends on the energy required for the reaction.

THE PROPERTIES OF ELECTROCATALYSTS FOR UREA SYNTHESIS

Characterization methods for urea detection and quantification

As discussed in the previous section, urea can be synthesized by the C-N coupling reaction of CO_2 with NO_2^-, NO_3^-, N_2, or NO. Side reactions are easy to occur during the catalytic process due to the complex multistep reaction mechanism. The competition of side reactions with synthesized urea results in low urea yields and FE. The detection of low urea concentrations is susceptible to various factors, leading to inaccurate quantification. Thus, both the influencing factors and detection limits of urea quantification need to be considered in urea synthesis. Currently, urea synthesized via electrocatalysis is primarily detected and quantified through colorimetry [including urease decomposition[35,42] and diacetyl monoxime (DAMO) method][29], ^{1}H nuclear magnetic resonance (NMR) spectroscopy[31] and high-performance liquid

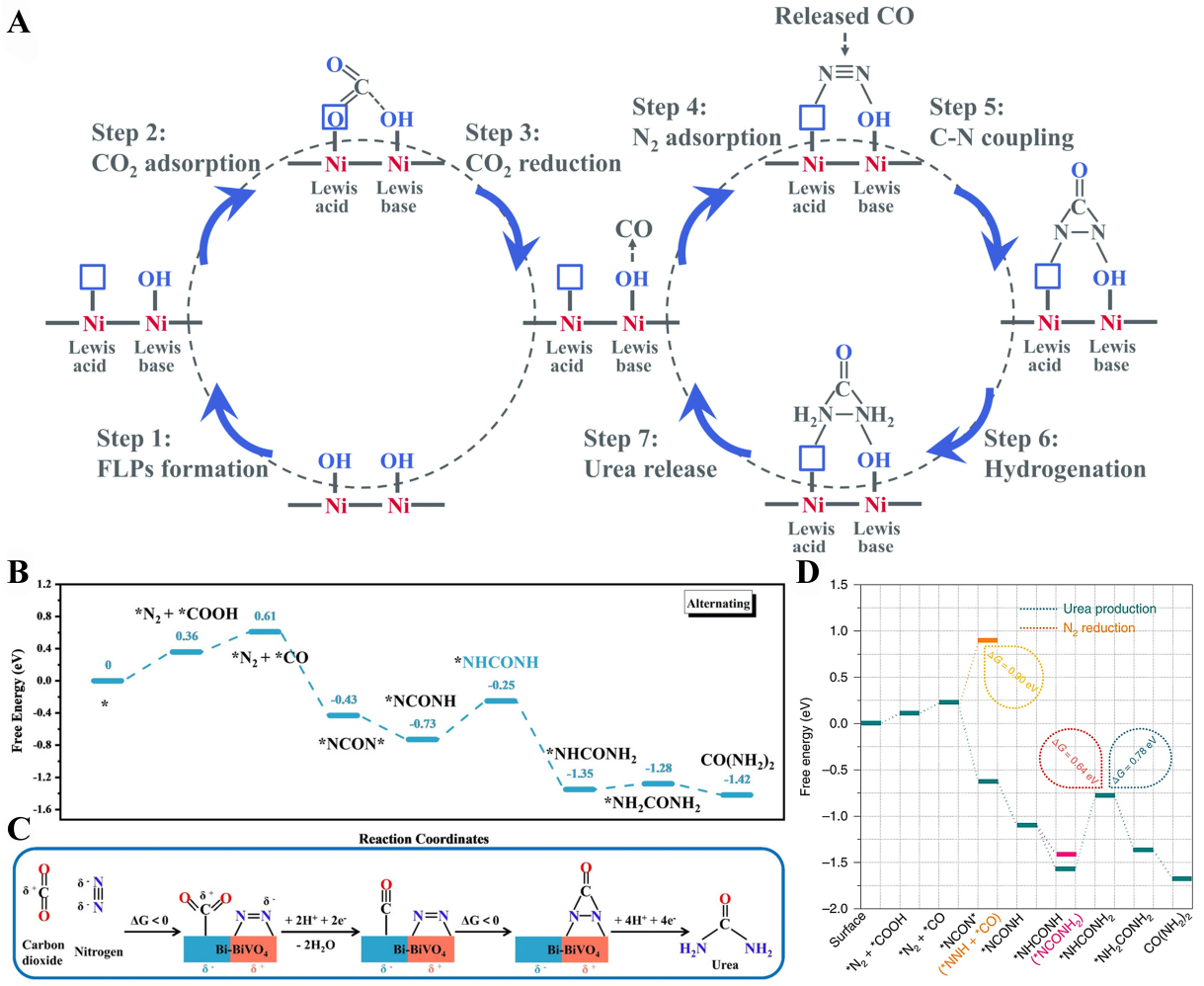

Figure 8. (A) Scheme of the simultaneous activation of N_2 and CO_2 to product urea under frustrated FLPs on $Ni_3(BO_3)_2$-150 catalysts. Reprinted with permission from ref[36]. Copyright 2021 The Royal Society of Chemistry; (B) Free energy of urea synthesis by alternate mechanism at Bi-$BiVO_4$; (C) Mechanism of urea electrosynthesis with the synergistic effect of the Bi-$BiVO_4$ Mott-Schottky heterostructure. Reprinted with permission from ref[39]. Copyright 2021 Wiley-VCH GmbH; (D) Free energy of urea synthesis at PdCu/TiO_2. Reprinted with permission from ref[13]. Copyright 2020 Nature Publishing Group. FLPs: Frustrated Lewis pairs.

chromatography-mass spectrometry (HPLC-MS)[23].

Urease decomposition method

The principle of urease decomposition method is that urease (urea amidohydrolase) has a catalytic reaction with urea in the electrolyte, hydrolyzing urea into NH_3 and CO_2 [given in Equation (4)]. The concentration of NH_3 in the solution after hydrolysis is measured using the indophenol blue method and ultraviolet and visible spectrophotometry (UV-vis). The final concentration of urea is then determined by calculation with Equation (5).

$$CO(NH_2)_2 + H_2O \xrightarrow{\text{urease}} 2NH_3 + CO_2 \quad (4)$$

$$c(\text{urea}) = \frac{c(NH_3, \text{after}) - c(NH_3, \text{before})}{2} \quad (5)$$

Huang *et al.* demonstrated that the urease decomposition method afforded a good linear relationship (R^2 = 0.999) with urea concentration in 0.2 M $KHCO_3$ electrolyte[43]. And the limit of detection (LOD) was 0.52 ppm. In addition, they explored the interfering factors in urea quantification. For example, the presence of NO_2^- may inhibit the production of indophenol derivatives, resulting in the underestimation of NH_4^+. The calculated values were smaller than the actual values. Ions such as Co^{2+}, Fe^{2+} and Mn^{2+} would repress the urease activity, leading to the underestimation of the calculated urea concentration. On the contrary, higher measurements would be obtained in the presence of Ru^{3+}, which could be attributed to the chemical reaction between Ru^{3+} and chromogenic reagent. Therefore, considering these interfering factors can effectively reduce the error and promote the accuracy of quantification when using the urease decomposition method.

DAMO method

Its principle is the reaction of urea and DAMO in an acidic solution containing ferric chloride and thiosemicarbazide. The colorimetric product formed by the reaction can be determined by UV-vis. In the work by Huang *et al.*, the method exhibited a LOD of 0.14 ppm in 0.2 M $KHCO_3$ electrolyte[43]. They also demonstrated that when the NO_2^- content in the electrolyte was higher than 20 ppm, using the DAMO method to quantify urea would exceed the acceptable error and lose its accuracy. Such interference phenomena were also present in reducing reagents such as S_2O_3, thiourea or thiosulfate which would cause redox reactions with the color reagent. Therefore, the DAMO method is not accurate enough when NO_2^- is used as an N source or when large quantities of NO_2^- exist in the electrolyte.

^{1}H NMR spectroscopy

^{1}H NMR method uses dimethyl sulfoxide-d_6 (DMSO-d_6) as a deuterated reagent. The un-post-processed electrolyte was thoroughly mixed with DMSO-d_6 and was then transferred into the NMR tube and tested using a Fourier transform NMR spectrometer. For the ^{1}H NMR method, the LOD was proved to be 0.54 ppm in 0.2 M $KHCO_3$ electrolyte[43]. It was gratifying that both the side reaction products and the metal ions leached from the catalyst had little effect on the quantification of urea due to the differences in the chemical environments of H atoms, which made the ^{1}H NMR spectroscopy a reliable quantification method.

HPLC-MS method

Compared to the ^{1}H NMR test, HPLC-MS can be used to characterize the urea without isotopic labeling, ^{13}C-labeled urea and ^{15}N-labeled urea. In 0.2 M $KHCO_3$ electrolyte, the LOD of the HPLC-MS was 0.42 ppm[43]. The quantification of urea would not be influenced by the presence of C-/N-containing by-products or other interfering substances.

Therefore, ^{1}H NMR and HPLC-MS methods are capable of accurately quantifying urea in most cases. Especially in the case of low urea yields, isotope labeling tests are reliable tools to ensure that the detected urea originates from electrocatalytic C-N coupling, rather than other impurities.

The main properties of electrocatalysts for urea synthesis

To overcome the disadvantage of the traditional urea synthesis process technology with high energy consumption, researchers have designed various kinds of electrocatalysts for the electrochemical synthesis of urea by compositional adjustment, structural design, elemental doping, and so on. And the selection of nitrogen sources, such as NO_3^-, NO_2^-, N_2, and NO, was expanded and co-reduced with CO_2 to achieve efficient electrochemical synthesis of urea. It is well known that FE is a performance index for evaluating urea production. By comparing the existing studies, it is not difficult to find that most of the catalysts that

took the construction of bimetallic sites as well as inducing the generation of OVs achieved good FEs. For example, Cu-Ti^{3+} sites reported by Cao *et al.*[21], Cu-W double sites by Zhao *et al.*[44], Co-Ru double sites in $SrCoRuO_3$ catalysts by Lv *et al.*[45] and the relay reaction of Zn and Cu in three-dimensional (3D) hybrid catalysts reported by Luo *et al.*[31]. The alternating and synergistic reaction mechanism of the dual sites reduced the possibility of C-C coupling, while the adsorption function of the OVs avoided the desorption of the intermediates to produce the unwanted by-products. Thus, the selectivity for urea electrosynthesis was improved. Additionally, Saravanakumar *et al.* constructed a three-phase reaction interface to improve the reaction efficiency by controlling the TiO_2 size to the nanometer level and constructing porous membranes with Nafion[46]. The $In(OH)_3$ and InOOH catalysts reported by Lv *et al.* effectively suppressed the HER and improved the urea selectivity through the n-to-p type transformation of the semiconductor behavior of the catalysts[29,30]. The main properties of electrocatalysts for the synthesis of urea are shown in Table 1.

DESIGN OF CATALYTIC SYSTEM

Metal system

In 1995, Shibata *et al.* realized the electrosynthesis of urea by constructing a Cu-loaded gas diffusion electrode for the first time[20]. The as-prepared catalyst simultaneously electrocatalyzed NO_2^- and CO_2 to urea and exhibited a current efficiency of about 37% at -0.75 V *vs.* reversible hydrogen electrode (RHE). After decades of development, metal system catalysts have made great progress. For example, Huang *et al.* used the *in situ* electrochemical reduction methods to construct the Zn NBs from ZnO nanosheets, and this catalyst successfully synthesized urea by simultaneous reduction of CO and NO, with a urea yield of 15.13 $mmol \cdot h^{-1} \cdot g^{-1}$ and FE of 11.26% at -0.92 V *vs.* RHE[27]. The high activity of Zn in urea synthesis was due to the intrinsic activity of metallic Zn and the control of nanostructures of the catalyst. The intrinsic activity could be described as the high selectivity for reducing CO_2 to CO and the inhibition of dimerization of $^*N$ intermediates during NO reduction reaction (NORR)[53]. The corresponding results of the characterization test and simulated calculation revealed that $^*CO$ and $^*NH_2$ (the critical intermediates in urea formation) were gained through the co-reduction of CO_2 and NO and coupled to form the C–N bond of urea step-by-step.

Recently, Liu *et al.* proposed an AuCu self-assembled nanofibers (AuCu SANFs) catalyst with a Boerdijk-Coxeter structure with (111)-dominant facets. The AuCu SANFs with one-dimensional nanostructure were used to couple the CO_2RR with NO_2^- to synthesize urea [Figure 9A-F][42]. In AuCu SANFs, abundant defects of AuCu 1D nanowires structure (twin boundaries, stacking faults, and atomic steps, shown in Figure 9D-F) provided plenty of highly active sites for electrocatalytic synthesis of urea[54], while the Boerdijk-Coxeter structure could bring the generation of lattice strain and modulability of electronic structure[55]. Combined with the synergistic effect of AuCu bimetal[56], the AuCu nanocatalyst synthesized urea with a yield of 3,889.6 $\mu g \cdot h^{-1} \cdot mg^{-1}_{cat.}$ at -1.55 V (*vs.* Ag/AgCl) and the maximum FE of 24.7%.

Similarly, Meng *et al.* used an electroreduction method to construct Cu@Zn nanowires with a self-supported core-shell structure, which was able to electrosynthesize urea by carbon dioxide and nitrate contaminants [Figure 9G][32]. This self-supported nanostructure was capable of avoiding using any of the polymer binders and increasing the active sites. The difference in work function between Cu and Zn led to the transfer of electrons from Zn to Cu, and the electron-deficient Zn surface would exhibit partial positive charge, which was more conducive to the electroreduction of NO_3^-[57]. The yield and FE of urea on Cu@Zn nanowires were apparently better than those on Zn and Cu catalysts. Combined with the characterization test and theoretical calculation, the results showed that the electron transfer between the Zn shell and the Cu core structure promoted the formation and coupling of $^*CO$ and $^*NH_2$ intermediates to generate C–N bonds, thereby improving electrocatalytic properties.

Table 1. The properties of electrocatalysts for the synthesis of urea

Nitrogen source	Catalysts	Electrolyte	Electrolytic cell	Voltage	Urea yield	FE/%	Cyclic stability	Ref.
NO_2^-	Cu-TiO_2-Vo	0.1 M $KHCO_3$ + 0.02 M KNO_2	H-cell	-0.40 V (*vs.* RHE)	20.8 μmol·h^{-1}	43.10	-	[21]
	Te-Pd NCs	0.1 M $KHCO_3$ + 0.01 M KNO_2	H-cell	-1.10 V (*vs.* RHE)	-	12.20	5 h	[22]
	Te-Pd NCs	0.05 M KNO_2	Flow cell	-1.20 V (*vs.* RHE)	-	10.20	5 h	[22]
	ZnO-Vo	0.2 M $NaHCO_3$ + 0.1 M $NaNO_2$	H-cell	-0.79 V (*vs.* RHE)	16.56 μmol·h^{-1}	23.26	15 h	[23]
	AuCu NFs	0.5 M $KHCO_3$ + 0.01 M KNO_2	H-cell	-1.55 V (*vs.* Ag/AgCl)	3,889.6 μg·h^{-1}·$mg^{-1}_{cat.}$	24.70	18 h	[42]
NO_3^-	TiO_2/Nafion	0.1 M KNO_3	H-cell	-0.98 V (*vs.* Ag/AgCl)	-	40.00	-	[46]
	$In(OH)_3$	0.1 M KNO_3	H-cell	-0.60 V (*vs.* RHE)	533.1 μg·h^{-1}·$mg^{-1}_{cat.}$	53.40	8 h	[29]
	InOOH-Vo	0.1 M KNO_3	H-cell	-0.50 V (*vs.* RHE)	592.5 μg·h^{-1}·$mg^{-1}_{cat.}$	51.00	10 h	[30]
	Cu@Zn	0.2 M $KHCO_3$ + 0.1 M KNO_3	H-cell	-1.75 V (*vs.* SCE)	7.29 μmol·cm^{-2}·h^{-1}	9.28	12 h	[32]
	Cu SACs	0.1 M $KHCO_3$ + 0.1 M KNO_3	H-cell	-0.90 V (*vs.* RHE)	4.3 nmol·s^{-1}·cm^{-2}	28.00	12 h	[33]
	Fe-Ni DASC	0.1 M $KHCO_3$ + 50 mM KNO_3/KNO_2	H-cell	-1.50 V (*vs.* RHE)	20.2 mmol·h^{-1}·g^{-1}	17.80	5 h	[34]
	Cu-CeO_2	0.1 M $KHCO_3$ + 50 mM KNO_3	H-cell	-1.60 V (*vs.* RHE)	52.84 mmol·h^{-1}·g^{-1}	5.29	4 h	[35]
	Fe(a)@C-Fe_3O_4/CNTs	0.1 M KNO_3	H-cell	-0.65 V (*vs.* RHE)	1,341.3 ± 112.6 μg·h^{-1}·$mg^{-1}_{cat.}$	16.50 ± 6.10	10 h	[47]
	$CuWO_4$	0.1 M KNO_3	H-cell	-0.20 V (*vs.* RHE)	98.5 ± 3.2 μg·h^{-1}·$mg^{-1}_{cat.}$	70.10 ± 2.40	10 h	[44]
	FeNi/NC	0.1 M KNO_3	H-cell	-0.90 V (*vs.* RHE)	496.5 μg·h^{-1}·$mg^{-1}_{cat.}$	16.58	6 h	[48]
	Zn/Cu	0.1 M $KHCO_3$ + 1,000 ppm KNO_3 [N]	Flow cell	-0.80 V (*vs.* RHE)	60 mmol·h^{-1}·g^{-1}	75.00	32 h	[31]
	Ru-CeO_2	0.1 M $KHCO_3$ + 50 mM KNO_3	H-cell	-0.70 V (*vs.* RHE)	20.2 mmol·h^{-1}·g^{-1}	20.10	8 h	[49]
	$SrCoRuO_3$	0.1 M KNO_3	H-cell	-0.70 V (*vs.* RHE)	1,522 μg·h^{-1}·$mg^{-1}_{cat.}$	34.10	12 h	[45]
N_2	$Ni_3(BO_3)_2$	0.1 M $KHCO_3$	H-cell	-0.50 V (*vs.* RHE)	9.70 mmol·h^{-1}·g^{-1}	20.36	20 h	[36]
	PdCu/TiO_2	0.1 M $KHCO_3$	Flow cell	-0.40 V (*vs.* RHE)	3.36 mmol·h^{-1}·g^{-1}	8.92	12 h	[13]
	Bi-$BiVO_4$	0.1 M $KHCO_3$	H-cell	-0.40 V (*vs.* RHE)	5.91 mmol·h^{-1}·g^{-1}	12.55	10 h	[39]
	Co-PMDA-2-mbIM	0.1 M $KHCO_3$	H-cell	-0.50 V (*vs.* RHE)	14.47 mmol·h^{-1}·g^{-1}	48.97	10 h	[50]
	$Sb_xBi_{1-x}O_y$	0.5 M K_2SO_4	H-cell	-0.30 V (*vs.* RHE)	307.97 μg·h^{-1}·$mg^{-1}_{cat.}$	10.90	20 h	[51]
	Ru-Pd/WO_3/MXene	0.5 M $NaNO_3$ + 0.5 M $NaHCO_3$	H-cell	-0.60 V (*vs.* RHE)	227 μg·h^{-1}·$mg^{-1}_{cat.}$	23.70	43 h	[52]
NO	Zn NBs	0.2 M $KHCO_3$	Flow cell	-2.10 V (*vs.* RHE)	15.13 mmol·h^{-1}·g^{-1}	11.26	5 h	[27]

FE: Faradaic efficiency; RHE: reversible hydrogen electrode; NCs: nanocrystals; NFs: nanofibers; SCE: saturated calomel electrode; SACs: single-atom catalysts; DASC: diatomic sites catalyst; PMDA: pyrodimethyl dianhydride; 2-mbIM: 2-methylbenzimidazole; Zn NBs: Zn nanobelts.

The latest breakthrough came from Luo *et al.*, who reported a 3D hybrid catalyst with functional synergy between Cu and Zn by spraying an incomplete Zn layer on top of the Cu layer [Figure 9H][31]. *In situ* spectroscopy and theoretical calculations demonstrated that Zn reduced the energy barrier for C-N coupling, and Cu lowered the reaction energy required for protonation to produce urea, realizing a relay electrocatalytic mechanism. By optimizing components and

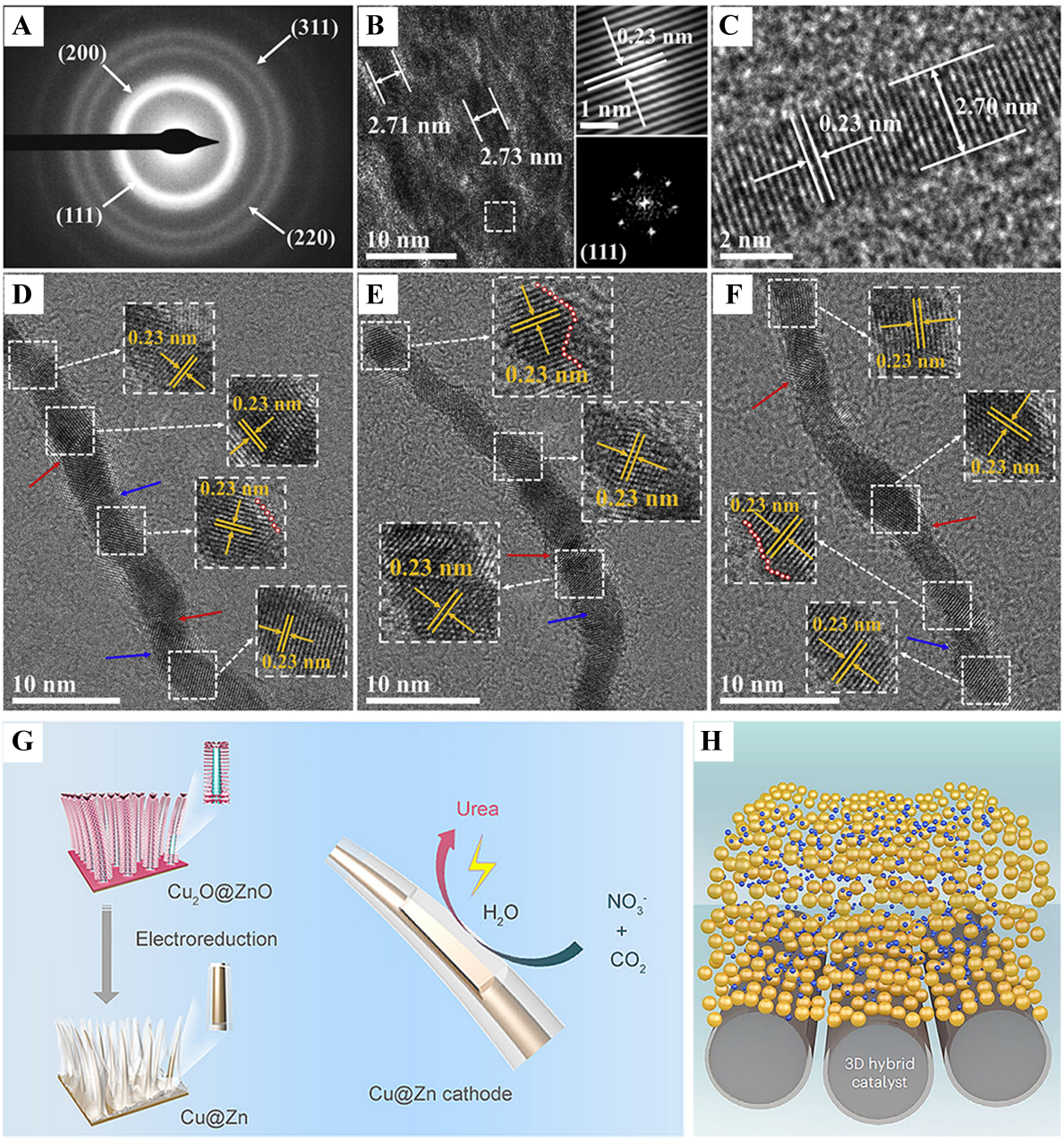

Figure 9. (A) SAED and (B) HRTEM for the AuCu self-assembled nanofibers. The illustrations in (B) show the lattice fringes of the square area and FFT pattern; (C-F) HRTEM for AuCu nanowires [red arrows (twin boundaries), blue arrows (stacking faults), and circles (atomic steps)]. Reprinted with permission from ref[42]. Copyright 2022 Elsevier; (G) Schematic illustration for the synthesis of Cu@Zn catalyst. Reprinted with permission from ref[32]. Copyright 2022 American Chemical Society; (H) Scheme of Zn/Cu 3D hybrid catalysts on a gas-diffusion layer. Orange and blue denote Cu and Zn, respectively. Reprinted with permission from ref[31]. Copyright 2023 Nature Publishing Group. SAED: Selected area electron diffraction; HRTEM: high-resolution transmission electron microscope; FFT: fast Fourier transform; 3D: three-dimensional.

electrochemical test configurations, the urea FE achieved an extraordinary 75% in simulated wastewater containing 1,000 ppm NO_3^- [N]. Hybrid catalysts, consisting of two types of sites - one that promoted C–N bond formation and another facilitated protonation, had the ability to avoid the need to balance the adsorption energies of all the essential steps using a single catalytic site. The Zn/Cu hybrid catalysts realized

a relay catalytic mechanism in which both the Zn and Cu sites were catalytically active and performed different functions. In contrast, single-component catalysts usually promote either the formation step of the C–N bond or the protonation step. For example, in the Cu@Zn core-shell catalyst described previously [Figure 9G], the shell layer Zn was catalytically active and its electronic structure was adjusted by the core layer Cu to promote C–N bond formation.

When it comes to the design of a metallic electrocatalyst, it is necessary to consider the intrinsic catalytic activity of the selected metal atoms. Priority should be given to the metal atoms with high CO_2RR and NRR selectivity. Nonetheless, the FE of pure metal catalysts was not universally high. The possible reason was that metal atoms were easy to aggregate, resulting in low atomic utilization and unclear catalytic active sites. Regulating the nanostructure of catalysts has been recognized as a universal method to optimize the catalytic performance of metal electrodes[58]. For example, the AuCu nanofiber catalyst synthesized by Liu was composed of ultrathin AuCu alloy nanowires. The nanowires arranged in parallel have the unique characteristics of anisotropy and high surface area, which can improve atomic utilization, accelerate electron transport, and avoid agglomeration and dissolution of catalysts. Cu@Zn nanowires developed by Meng had unique self-supported nanostructures that avoided the use of polymer binders and effectively increased the active sites on the catalyst. What is more, the electronic interactions between components would be promoted by metal alloying. On the AuCu SANFs catalyst designed by Liu *et al.*, the binding of Au changed the coordination and electronic structure of Cu, enhancing the adsorption and activation of CO_2 and improving the catalytic selectivity[42]. Lu *et al.* took advantage of the difference in work functions between Cu and Zn to construct an electron-deficient Zn surface, facilitating the electrical reduction of NO_3^- and increasing the opportunities for C-N coupling. Thus, the performance of bimetallic catalysts was generally better than that of single metals[59].

Metallic oxide system

In 2017, through two distinct methods, co-precipitate and microwave, Siva *et al.* constructed two structurally different $FeTiO_3$ electrodes as high-efficiency catalysts for CO_2 and NO_2 reduction to urea at a low current density of 10 mA·cm^{-2}[60]. It was observed that the performance of Fe-doped TiO_2 was more favorable than Cd or Co in improving the conversion of CO_2 and NO_2 to urea. Although the work by Siva *et al.* only studied the performance of the catalyst from the potential instead of urea synthesis yield and FE, through the comparison of the two catalytic electrodes synthesized by different methods, we learned that the $FeTiO_3$ catalyst synthesized by microwave possessed a more uniform crystal structure, which provided more adsorption functional groups[60]. Therefore, microwave synthesized $FeTiO_3$ showed better cathodic behavior than co-precipitate synthesized $FeTiO_3$ for urea synthesis.

Saravanakumar *et al.* constructed the electrocatalyst by drop-casting the P-25 TiO_2 nanoparticles and Nafion solution on the electrode[46]. TiO_2 had the characteristics of high oxidation/reduction capacity and high structural stability, and could be combined with Nafion to form a stable porous film on the electrode surface, creating a balanced three-phase reaction interface, which was favorable for urea synthesis[61]. As expected, the prepared TiO_2/Nafion nanocomposite electrode successfully converted CO_2 and NO_3^- to urea with a FE of 40% at a lower overpotential than that reported by similar systems previously.

After the creative work on realizing C-N coupling and producing acetamide with excellent selectivity and efficiency that used ammonia as the N source by Jouny *et al.* in 2019[16]. Chen *et al.* proposed that the co-reduction of nitrogen and carbon dioxide could form the C–N bonds, thus achieving urea synthesis under ambient conditions [Figure 10A-C][13]. They demonstrated an approach to construct an electrocatalyst by attaching PdCu alloy nanoparticles to TiO_2 nanosheets to the electrocatalytic coupling of N_2 and CO_2 in

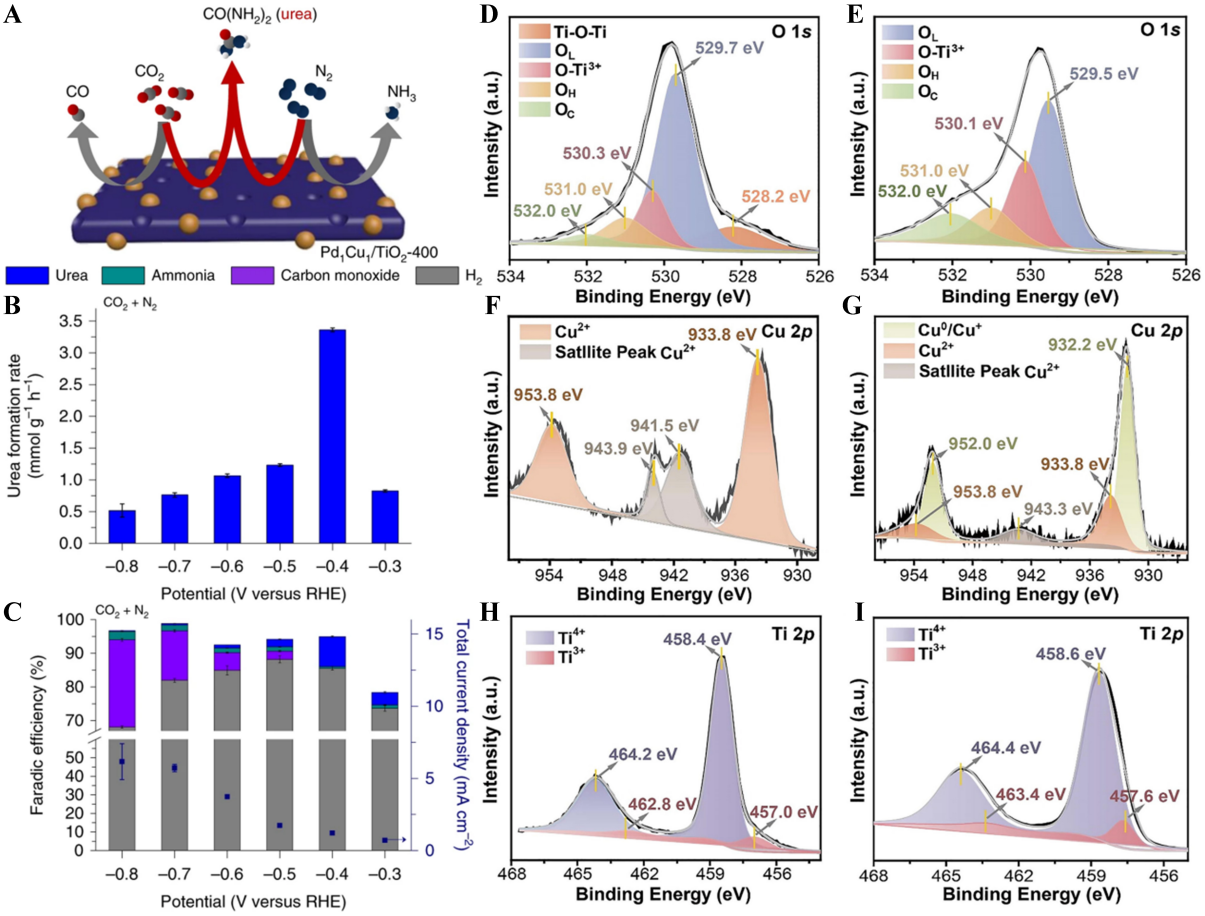

Figure 10. (A) Urea synthesis schematic diagram at Pd_1Cu_1/TiO_2-400; (B) Formation rate of urea at Pd_1Cu_1/TiO_2-400; (C) The current density and FE for each product at different potentials at Pd_1Cu_1/TiO_2-400. Reprinted with permission from ref[13]. Copyright 2020 Nature Publishing Group; (D and E) O 1s XPS of (D) TiO_2 without doping and (E) Cu-TiO_2; (F and G) Cu 2p XPS of (F) CuO and (G) Cu-TiO_2; (H and I) Ti 2p XPS of (H) TiO_2 without doping and (I) Cu-TiO_2. Reprinted with permission from ref[21]. Copyright 2020 Elsevier Inc. FE: Faradaic efficiency; XPS: X-ray photoelectron spectroscopy spectra.

water and form urea. Compared to the single-metal-loaded catalyst, Pd_1Cu_1/TiO_2 exhibited higher urea yield and FE, and a decline in the onset potential. The improvement of catalytic performance could be attributed to the optimization of the electronic structure and the strong interaction between the bimetals and the support. TiO_2 nanosheets treated with a reduction atmosphere at elevated temperatures were easy to form OVs. The formation of OVs was capable of narrowing the band gap of TiO_2 without changing the crystalline phase of the materials. Moreover, the comparison experiment proved that the interaction between TiO_2 and metal was stronger than that of carbon support (Carbon Black XC72R). The TiO_2 had been reported to stabilize the intermediates to promote CO_2RR[62]. However, the N_2 with low solubility and the stable N≡N triple bond (940.95 kJ·mol^{-1}) resulted in poor selectivity, FE, and yield of urea[63]. CeO_2 is an n-type semiconductor with high electron density that can stabilize metal dopants. According to this, Wei *et al.* reported a catalyst loaded with Cu single atoms on a CeO_2 carrier synthesized by wet impregnation and calcination[35]. A series of characterization proved that in comparison to the high concentration Cu-doped sample H-Cu-CeO_2, the low concentration Cu-doped L-Cu_1-CeO_2 exhibited a nanorod morphology with atomically dispersed atoms, which provided active sites that could be accurately identified. The catalyst reached an average urea yield rate of 52.84 mmol·h^{-1}·g$^{-1}_{cat.}$ at -1.60 V (*vs.* RHE), which was at the leading level among similar studies reported so far. In order to monitor the structural evolution of the Cu_1-CeO_2 catalyst

during the C-N coupling process, this work employed the Operando X-ray absorption spectroscopy (XAS) technique. The XAS results indicated that during the catalytic process, the individual Cu^{2+} was gradually reduced to Cu^{+} and Cu^{0} to form Cu_4 clusters which were the real active sites for electrocatalytic urea synthesis. This process was reversible at open-circuit potential, thus providing the catalyst with superior structural and electrochemical stabilities. Yu *et al.* attempted to use Ru-doped CeO_2 to increase the OV concentration, and successfully doped Ru into the interior of the CeO_2 lattice through a wet reduction process[49]. Ru atoms partially replaced the Ce sites, leading to lattice contraction, resulting in local lattice disorder and promoting the formation of OVs. OVs could promote the electroreduction of NO_3^- and CO_2 through enhanced adsorption, and Ru could capture the $^*CO$, leading to significant inhibition of HER. The synergistic effect of Ru doping and OVs optimized the adsorption and activation of the reactants and facilitated the C-N coupling kinetics. At a Ru doping ratio of 5%, the catalyst had a high urea yield (20.2 $mmol \cdot h^{-1} \cdot g^{-1}$) and FE (20.1%) at a low overpotential (-0.70 V *vs.* RHE).

As mentioned above, OVs are important structural defects in metal oxides. It is rich in electron density and can act as a catalytic center[64]. Studies have shown that OVs would induce anatase $TiO_2(101)$ surface to form a pair of Ti^{3+} sites, which exhibited excellent binding and reduction capacity for nitrogen atoms[65]. Therefore, Cao *et al.* adulterated Cu in TiO_2 (Cu-TiO_2) to promote the forming of abundant defect sites and OVs [Figure 10D-I][21]. The doped Cu acted as the main adsorption site for CO_2 and provided electrons to form $^*CO$ intermediates. At the same time, the low-valence Cu dopants induced abundant OVs, which were conducive to the formation of exposed bi-Ti^{3+} active sites. Adsorption and reduction of NO_2^- on Ti^{3+} sites elevated the selectivity of NO_2^--to-$^*NH_2$[66]. The synergistic interaction of the two sites promoted the formation of $^*CO$ and $^*NH_2$ intermediates and led to efficient C-N coupling subsequently. This Cu-TiO_2 electrocatalyst with rich OVs exhibited a fabulous urea production rate (20.8 $\mu mol \cdot h^{-1}$) at -0.40 V (*vs.* RHE) with a FE of 43.1%, significantly better than those of TiO_2 without doping (5.91 $\mu mol \cdot h^{-1}$ and 27.3%). After that, Meng *et al.* designed a self-supported ZnO porous nanosheet with rich OVs (ZnO-V), and used it as an electrocatalyst for efficient urea synthesis with carbon dioxide and nitrite as raw materials[23]. Due to the presence of surface oxygen-rich vacancies, the urea yield of ZnO-V reached 16.56 $mmol \cdot h^{-1}$ at -0.79 V(*vs.* RHE), obviously better than that of ZnO (7.72 $mmol \cdot h^{-1}$). And the FE of ZnO-V achieved 23.26%, which was approximately three times as high as that of ZnO (8.10%). Lv *et al.* used a sol-gel chemical process and controlled thermal treatment to synthesize $SrCoRuO_3$ catalysts with Co-Ru double sites[45]. Meanwhile, the co-doping produced abundant OVs, which modulated the electronic structure of the active sites, realizing efficient urea electrosynthesis. The substitution of Ru sites by Co could distort the $SrRuO_3$ crystal structure due to the smaller atomic radius of Co. In their work, tunable lattice strain was realized by precise control of Co doping ratio. Ru and Co atoms had been demonstrated to be active metals for NO_3^- and CO_2 activation, respectively. *In situ* experiments and DFT theoretical calculations indicated that Co and Ru acted as active sites for the formation of $^*CO$ and $^*NH_2$ intermediates, respectively. The OVs modulated the electronic structure of Co and Ru sites, weakening the adsorption of the key intermediates. The synergistic effect of Co-Ru sites and OVs promoted the C-N coupling between $^*CO$ and $^*NH_2$, avoiding the desorption of the intermediates to produce unwanted by-products.

In addition to the introduction of OVs in the electrocatalyst, the urea yield can also be increased by designing the heterojunction on the electrocatalyst. For example, Yuan *et al.* designed the Bi-$BiVO_4$ electrocatalyst with Mott-Schottky heterostructures, which reached an excellent yield rate of urea of 5.91 $mmol \cdot h^{-1} \cdot g^{-1}$ at -0.40 V *vs.* RHE and a FE of 12.55% [Figure 11A-F][39]. This might be attributed to the fact that the formed heterostructure structure interface could promote charge transfer spontaneously; the resulting space-charge layer guaranteed the selective adsorption of CO_2, activation of inert N_2, and the exposure of more active sites, contributing to C-N coupling and urea synthesis[40]. The electrochemical

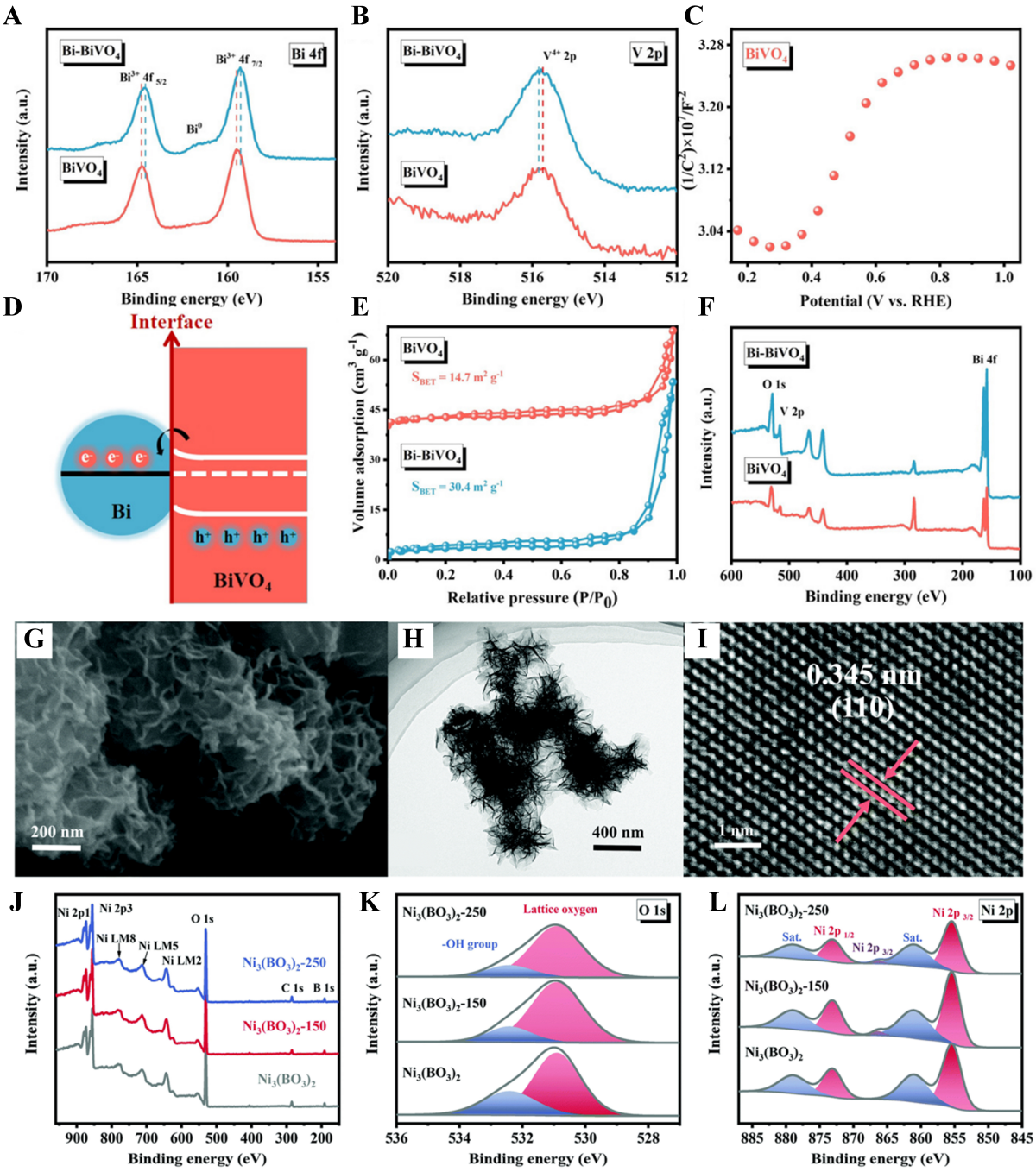

Figure 11. (A) High-resolution Bi 4f and (B) V 2p spectra for $BiVO_4$ and Bi-$BiVO_4$; (C) Mott-Schottky diagram for $BiVO_4$; (D) Diagram of charge transfer process at Bi-$BiVO_4$; (E) Specific surface area and (F) XPS for $BiVO_4$ and Bi-$BiVO_4$. Reprinted with permission from ref[39]. Copyright 2021 Wiley-VCH GmbH; (G) SEM and (H and I) HRTEM images for $Ni_3(BO_3)_2$-150 catalysts; (J) XPS survey spectra, (K) high-resolution O 1s and (L) Ni 2p spectra for the original $Ni_3(BO_3)_2$, $Ni_3(BO_3)_2$-150, and $Ni_3(BO_3)_2$-250. Reprinted with permission from ref[36]. Copyright 2021 The Royal Society of Chemistry. XPS: X-ray photoelectron spectroscopy spectra; SEM: scanning electron microscopy; HRTEM: high-resolution transmission electron microscope.

impedance spectroscopy (EIS) showed that the Bi-$BiVO_4$ had a smaller semicircle and a higher slope than the unhybrid $BiVO_4$, confirming the formation of the localized nucleophilic and electrophilic regions on the surface of Bi-$BiVO_4$. Theoretical simulations verified that electron-rich N atoms in N_2 and electron-deficient

C atoms in CO_2 would be targeted for adsorption in the electrophilic and nucleophilic regions, respectively. Govindan *et al.* successfully doped Ru-Pd alloy nanoparticles into two-dimensional (2D) WO_3 and MXene nanosheets to form a Ru-Pd/WO_3/MXene heterostructure[52]. A bifunctional electrode was constructed for simultaneous cathodic reduction of CO_2 and N_2 to urea and anodic oxidation of water. In the electrochemical reduction process at the cathode, CO_2 was first converted to $^*CO$ and then directly coupled with N_2 via sequential protonation to produce urea. At -0.60 V (*vs.* RHE), the urea yield was 227 $\mu g \cdot h^{-1} \cdot mg^{-1}_{cat.}$ with a FE of 23.7%. Since WO_3 was at a lower conduction band (CB) position, it could adsorb single pairs of N_2 in the active site more efficiently, thus activating the reduction of N_2 to $^*N_2$ intermediates. The 2D structure of MXene provided a stable platform for catalytic activity and excellent conductivity. The construction of the Ru-Pd metal active sites in the WO_3/MXene heterostructure increased the solubility of CO_2, which was converted to $^*CO$ intermediates by the electron-proton transfer process. Therefore, the Ru-Pd/WO_3/MXene catalyst had an efficient C-N coupling capability.

Nevertheless, the above strategy only focused on the adsorption and activation of reactant molecules, while ignoring the electrocatalytic C-N coupling reaction that occurred during urea synthesis. Therefore, Yuan *et al.* further synthesized the floral nickel borate [$Ni_3(BO_3)_2$] by designing unique frustrated FLPs [Figure 11G-L][36]. FLPs consisting of LA and LB enabled chemisorption and reaction of gas molecules[67]. On the $Ni_3(BO_3)_2$ catalyst, the coordination unsaturated Ni sites and the neighboring surface hydroxyl groups acted as LA and LB sites, respectively. During the reaction, the LA sites coupled with empty orbitals would capture the lone pair electrons from the N atoms in N_2, while the surplus electrons in the LB sites would be donated to the C atoms in CO_2. On the FLPs, the unoccupied orbitals of LA and the non-bonding orbitals of LB would interact with the bonding and antibonding orbitals of the reactant molecules, respectively, which led to the polarization of N_2 and CO_2. After molecular activation via FLPs, the $^*N{=}N^*$ intermediate was coupled with the $^*CO$ intermediate through an σ-orbital carbonylation way to synthesize the $^*NCON^*$ precursor[37,68]. The acquired highest yield rate was 9.70 $mmol \cdot h^{-1} \cdot g^{-1}_{cat.}$ and the FE was 20.36% at -0.50 V (*vs.* RHE).

A new study by Chen *et al.* doped Sb in amorphous BiO_x clusters, which affected the mode of CO_2 adsorption by modulating the 6p orbital configuration of Bi, improving the possibility of producing urea[51]. The prepared $Sb_xBi_{1-x}O_y$ clusters possessed a reaction potential of only -0.30 V (*vs.* RHE), a yield of 307.97 $\mu g \cdot h^{-1} \cdot mg^{-1}_{cat.}$, and a FE of 10.9%, which was considerably improved in performance compared to the undoped BiO_x clusters (80 $\mu g \cdot h^{-1} \cdot mg^{-1}_{cat.}$, FE = 1.3% at -0.40 V *vs.* RHE). Both *in situ* experiments and the first principles calculations indicated that Sb was capable of effectively stabilizing the electronic and geometrical structures of amorphous BiO_x clusters. The doping of Sb introduced an OV in the BiO_x system, corresponding to two excess electrons localized in the 6p orbital of Bi, and the low-oxidation state of Bi(II) emerged[69]. During catalyzing, the specific Bi-O coordination number of Bi(II) decreased and stabilized at ~1.4, and these unsaturated coordination sites had high catalytic activity. As a result, the adsorption geometry of CO_2 on the catalyst surface was changed from O-connected to C-connected, and the preferential adsorption of C atoms promoted the generation of the key $^*CO$ intermediates of C-N coupling while obstructing the formation of unwanted by-products, such as HCOOH derivatives. Furthermore, the Bi(II) active sites could facilitate C-N coupling by efficiently injecting electrons into N_2 that favorably modified the symmetry of the CO_2 and N_2 frontier orbitals. DFT calculations showed that the $^*N_2$ with injected electrons formed a "new-type" highest occupied molecular orbital (HOMO) that matched the symmetry of the lowest unoccupied molecular orbital (LUMO) of $^*CO$. Then, the possibility of forming $^*NCON^*$ by C-N coupling was greatly enhanced.

The catalysts of metal oxide systems are usually doped with metal atoms to achieve the electrocatalytic synthesis of urea. Therefore, the selection of a suitable substrate material should be taken into account primarily. The chosen substrate ought to generate strong interactions with the doped metal, and it is necessary to ensure that the loaded heteroatoms are sufficiently well dispersed. Secondly, designing active sites that combine the abilities of adsorption, synergistic activation and C-N coupling of reactant molecules is desirable. For instance, Zhao *et al.* utilized the high-valent metals W and Cu to prepare a $CuWO_4$ catalyst with alternating reaction sites[44]. An outstanding FE of 70.1% ± 2.4% was achieved at a low overpotential of -0.20 V (*vs.* RHE). It is well known that Cu is a common CO_2RR catalyst, but consecutive Cu sites on Cu-based catalysts may generate C-C coupling which reduces the synthesis efficiency of urea. High-valent tungsten oxides are beneficial for stabilizing $^*NO_2$ intermediates and do not trigger CO_2 reduction reactions. So, the alternating reaction site composed of W and Cu, two active sites with different functions, could effectively balance the adsorption capacity of $^*NO_2$ and $^*CO$ intermediates. In addition, defect engineering has been widely applied to modulate the physical and chemical properties of catalysts. OVs are accessible and significant structural defects in metal oxides that can serve as active sites with abundant electrons. For example, in Cu-TiO_2 catalysts, the doping of low-valent Cu induced abundant OVs, favoring the formation of exposed bi-Ti^{3+} active sites[21]. ZnO with OVs (ZnO-V) exhibited higher electrochemically active surface area (ECSA) than pure ZnO[23]. What is more, research by Yuan *et al.* provides the idea of utilizing heterojunction to induce spontaneous charge transfer and generate space-charge regions[39]. The engineering of distinct space-charge regions is capable of guiding the accurate adsorption and activation of reactant molecules, which contribute to the thermodynamically feasible coupling of the C–N bond and efficient urea production.

Metal hydroxide system

N-type semiconductor catalysts have been used in the electrosynthesis of urea due to their properties of inhibiting the HER[70]. Thus, Lv *et al.* realized urea electrosynthesis via directly coupling NO_3^- with CO_2 on an $In(OH)_3$ catalyst with {100} facets at ambient conditions[29]. The synthesized catalyst achieved highly selective urea production with a yield of 533.1 $\mu g \cdot h^{-1} \cdot mg^{-1}_{cat.}$ and FE of 53.4% at -0.60 V (*vs.* RHE). It is noted that the selectivity of nitrogen and carbon was 82.9% and nearly 100%, respectively. This study showed that the CO_2 absorbed at the surface, in addition to being the feedstock for the urea synthesis, could also help produce the hole accumulating layer on the catalyst by trapping electrons, resulting in an n-to-p type transformation of the semiconductor behavior of the $In(OH)_3$ surface. The inhibition of HER was achieved by the transformation of n-p semiconductor properties on the surface of $In(OH)_3$ electrocatalyst[71].

On this basis, Lv *et al.* synthesized the OV-rich indium oxyhydroxide electrocatalyst (Vo-InOOH)[30]. The DFT calculations indicated that the rate-determining step in the whole urea synthesis process was the $^*CO_2NH_2$ protonation. The defect engineering of Vo could reconfigure the electronic structure of the surface in the active site, thereby reducing the energy barrier for converting $^*CO_2NH_2$ to $^*COOHNH_2$, which was the determining factor of the catalytic efficiency in this system. The constructed Vo-InOOH electrocatalyst showed a remarkable FE of 51.0%, with a yield of 592.5 $\mu g \cdot h^{-1} \cdot mg^{-1}_{cat.}$.

Since the steps to synthesize urea are sequential protonation processes after the C-N coupling, the inhibition of the HER is of great significance to the overall efficiency. Lv *et al.* ingeniously utilized the manipulated conversion of semiconductor properties on the indium oxyhydroxide surface to achieve effective inhibition of the HER[29]. Despite many debates about the mechanism of n-p conversion in semiconductors, the concept of controlling electron transfer still inspires us to design more efficient electrocatalyst surfaces that facilitate C-N coupling reactions.

Nitrogen-doped carbon system

The system that doped heteroatoms (e.g., N) on the carbon substrate had drawn attention as an electrocatalyst due to their unique 2D nanostructure, high surface area, and more exposed active sites[72]. In 2021, Roy *et al.* first proposed dual-Si doped graphene-C_6N_6 sheets (Si_2-g-C_6N_6) and used theoretical calculation of DFT to study the process of N_2 and CO_2 coupling[73]. Bader charge analysis indicated that the charge transferred from the doped surface to the antibonding π^* orbitals of the N_2. The elongation of the N–N bond led to the activation of the N_2. The activated N_2 spontaneously adsorbed the *CO intermediate to form a C-N coupling. Moreover, according to DFT calculations, protons were more likely to be adsorbed at the Si active sites instead of the free N centers of the sheet. Thus, the potential of urea production initially was far lower than that of NH_3 synthesis and HER. Similarly, Dutta *et al.* proposed metal-free electrocatalysts based on dual silicon-doped C_9N_4 nanosheets, which could effectively produce urea with a low overpotential value [Figure 12A-C][74]. According to the Bader charge analysis, the presence of diatomic Si on the C_9N_4 substrate generated surplus surface charge density that could be provided to adjacent N atoms from N_2. Thus, the Si sites became the active center for N_2 catalysis, adsorbing N_2 in a side-on manner. Compared to *NHH, the density of states images of *N(CO)N had more overlap around the Fermi level, illustrating that the interaction between Si and attached N was stronger. Hence, the formation of *N(CO)N was more favorable, which meant the synthesis of urea was more favorable. Both above studies had shown that metal-free C_xN_y materials could promote PCET reactions, where CO was inserted into activated N_2 and then directly coupled to C–N bonds to form *NCON*, which was an important intermediate for urea production.

Single-atom catalysts loaded on carbon substrates exhibited exceptional electrocatalytic activities because of the unique electronic structure and maximized atom utilization[75]. Leverett *et al.* designed a Cu single-atom catalyst (Cu-SAC) in the carbon framework that doped with N, which was able to electrocatalyze both CO_2RR and NO_3^-RR [Figure 12D-F][33]. The electrochemical measurements showed that the CO FE of the coordination structure of Cu-N_4 was much higher than that of Cu-N_{4-x}-C_x. The polarization curves for CO_2RR also demonstrated that the intrinsic activity of CO_2RR at the Cu-N_4 site was significantly higher. Compared with Cu-N_3-C_1 and Cu-N_2-C_2, Cu-N_4 had a lower Gibbs free energy (ΔG) of *COOH formation according to the DFT calculations. In addition, Cu-N_4 had almost no decrease in CO FE at more negative potentials, which could be attributed to the enhanced coupling of $^*CO_2$ and $^*NO_2$, resulting in improved urea yields. The performance of the urea production rate reached 4.3 nmol·s^{-1}·cm^{-2}, and the urea FE was 28% at -0.90 V (*vs.* RHE).

The adjacent sites of bimetallic atoms have the ability to manipulate the geometric and electronic structures of SACs[76]. Zhang *et al.* pioneered the bonding of Fe-Ni pairs to prepare bonded Fe-Ni diatomic catalysts (B-FeNi-DACs) [Figure 13][34]. The DFT computations demonstrated that in the single-atom doping system, the active center was covered by the *NO intermediates, which inhibited the effective capture and activation of CO_2. After the doping of the second metal atom, the applied potential required to drive *CO generation was reduced, which indicated that the bimetallic sites were more effective in promoting C-N coupling. The bonded Fe-Ni pairs acted as the active sites for synergistically adsorbing and activating of reactants, promoting the thermodynamically and kinetically of C-N coupling[77]. At -1.50 V *vs.* RHE, an excellent urea yield rate of 20.2 mmol·h^{-1}·g^{-1} had been successfully realized with an FE of 17.8%. Identically, the latest research reported by Hou *et al.* also emphasized the feasibility of urea production through C-N coupling on alloy catalysts[48]. Considering the excellent performance of nickel-based catalysts in CO_2RR and iron-based catalysts in NO_3^-RR[78,79], Hou *et al.* constructed bimetallic $FeNi_3$ alloy particles loaded with N-doped porous carbon for electrocatalytic urea synthesis by reduction of CO_2 and NO_3^-[48]. The structure of porous carbon promoted electrochemical kinetics, as well as the sufficient exposure of active sites. The prepared electrocatalysts achieved the highest yield of 496.5 μg·h^{-1}·mg$^{-1}_{cat.}$ with a FE of 16.58% at -0.90 V (*vs.* RHE).

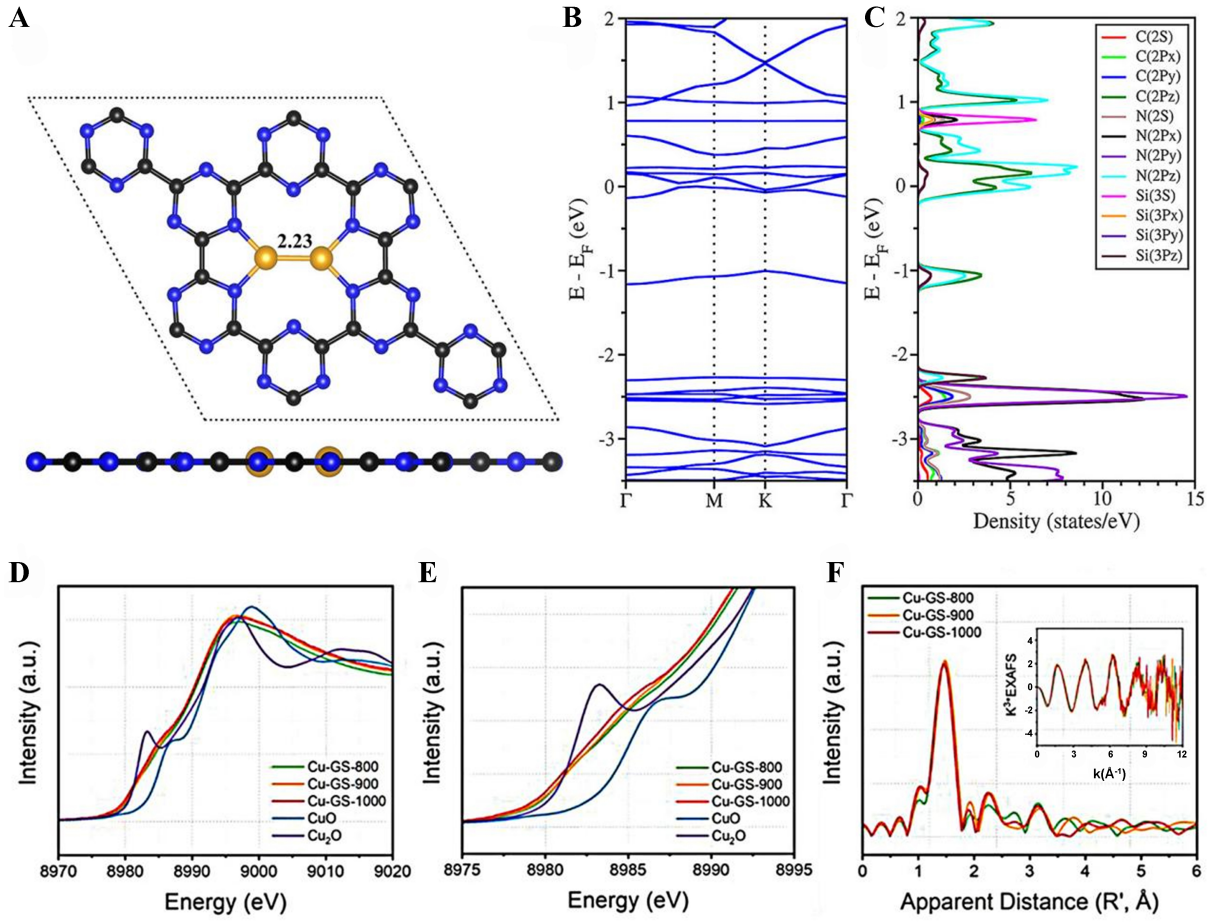

Figure 12. (A) Optimized geometry for the surface of Si_2-g-C_6N_6 (black ball: C atom, blue ball: N atom, golden ball: Si atom, and numerical value shows the bond length, Å); (B) HSE03 band structure and (C) Projected density of state for the Si_2-g-C_6N_6 surface. Reprinted with permission from ref[73]. Copyright 2021 American Chemical Society; (D and E) XANES spectra at Cu K-edge for Cu single atoms confined in graphene sheets (Cu-GS-800, 900 and 1000), compared with $Cu^{II}O$ [Cu(II)] and Cu^{I}_2O [Cu(I)]; (F) Fourier transformed EXAFS at the Cu K-edge for Cu-GS-800, 900 and 1000. Reprinted with permission from ref[33]. Copyright 2022 The Authors. Advanced Energy Materials published by Wiley-VCH GmbH. XANES: X-ray absorption near edge structure; EXAFS: extended X-ray absorption fine structure.

Zhu *et al.* proposed that the MN_3-M'N_4 bimetallic moiety with two dispersed active sites could simultaneously inhibit the separate reduction process after the adsorption of CO_2 and N_2[80]. They used ab initio molecular dynamics (AIMD) simulations to calculate the thermal stability of 26 homonuclear and 650 heteronuclear bimetallic systems and filtered out 205 structurally stable combinations. And then they picked out 18 M-M' combinations (Sr-Ir, Ti-Rh, Fe-Os, Y-Co, Y-Rh, Zr-Rh, Sc-Os, Cr-Ir, Mn-Rh, Mn-Ir, Co-Os, Y-Fe, Y-Ru, Zr-Ru, Y-Re, Y-Ir, Zr-Cr, Ru-Co) with high catalytic activity by a five-step high-throughput screening on the basis of NCON, CO and OCOH pathway. Combined with the evaluation of urea synthesis selectivity, the three most superior M-M' (Fe-Os, Co-Os and Ru-Co) electrocatalysts were finally obtained. Among them, the Ru-Co combination (RuN_3-CoN_4) exhibited a very low limiting potential and excellent urea production performance, which had great potential for practice.

Synthesizing monatomic or diatomic catalysts on the carbon nitride substrates was a significant strategy to improve the utilization of atoms[81,82]. In this system, the coordination structures of active sites become a key factor that affects the catalytic efficiency. The bonded diatomic catalysts not only overcome the limitation

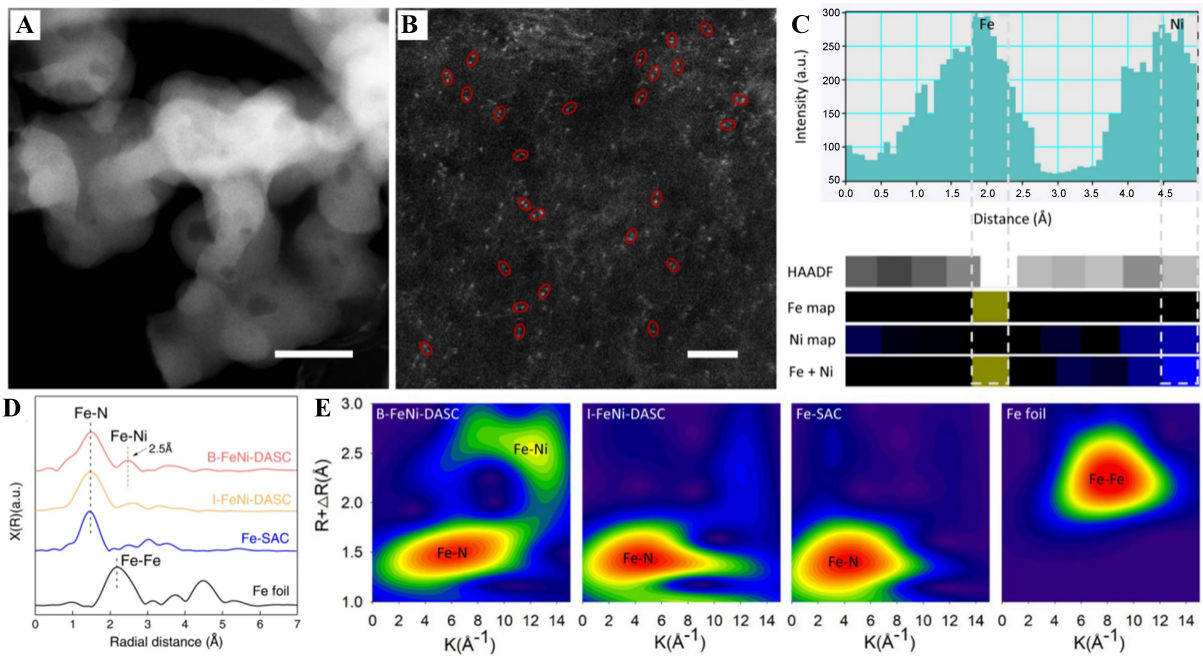

Figure 13. (A) TEM (The scale bar is 100 nm) and (B) Aberration-corrected HAADF-STEM of B-FeNi-DASC. (The scale bar is 2 nm); (C) HAADF-STEM intensity profile with atomic-resolution EELS for the Fe-Ni pair; (D) Fourier transform EXAFS for Fe-SAC, I-FeNi-DASC, and B-FeNi-DASC; (E) Wavelet-transform of Fe element for Fe foil, Fe-SAC, I-FeNi-DASC, and B-FeNi-DASC. Reprinted with permission from ref[34]. Copyright 2022 Nature Publishing Group. TEM: Transmission electron microscopy; HAADF-STEM: high-angle annular dark-field-scanning transmission electron microscopy; B-FeNi-DASC: bonded Fe-Ni diatomic sites catalyst; EELS: electron energy loss spectroscopy; EXAFS: extended X-ray absorption fine structure; SAC: single-atom catalyst.

that single-atom catalysts selectively adsorb and activate reactants unilaterally, but also increase the possibility of C/N intermediates meeting and coupling to form critical C–N bonds. The construction of diatomic sites has emerged as a viable strategy to achieve synergistic adsorption and activation for electrocatalytic C-N coupling reactions, which improve the yield and FE of urea effectively[83].

Other system

Metallophthalocyanine

Based on the gas diffusion electrode, Shibata *et al.* devoted to the studies of metallophthalocyanine (M-Pc, M = Cr, Mo, Mn, Ru, Co, Rh, Ir, Ni, Pd, Pt, Cu, Ag, Au, Zn, Cd, In, Tl, Sn, and Pb) catalysts[84]. A series of studies indicated that Co-Pc, Ni-Pc, and Pd-Pc catalysts showed high current efficiency of urea formation. Among them, the Ni-Pc catalyst exhibited a maximum current efficiency of approximately 40% at -1.50 V. It was discovered that the capacity of the catalyst to create urea is contingent on its ability to produce CO and NH_3. Moreover, in another report by Yang *et al.*, it was proved that when NO_3^- cannot be reduced to nitrite ions and ammonia, urea product could not be obtained on the M-Pc (M = Ti, V, Cr, Mo, Fe, Ru, Co, Ni, Pd, Cu, Zn, Cd, Ga, In, Ge, Sn, and Pb) gas diffusion electrode[85].

Platinum electrode coated polymer

As early as 2016, Kayan *et al.* realized the electrocatalytic reduction of CO_2 and N_2 on platinum electrodes coated with polyaniline (PAni) and polypyrrole (PPy) in 0.1 M Li_2SO_4/0.03M H^+ aqueous solution at -0.325 V [*vs.* normal hydrogen electrode (NHE)][86]. After 5 h electrolysis time, 21.2 and 12 μmol of urea were produced on PAni and PPy, respectively.

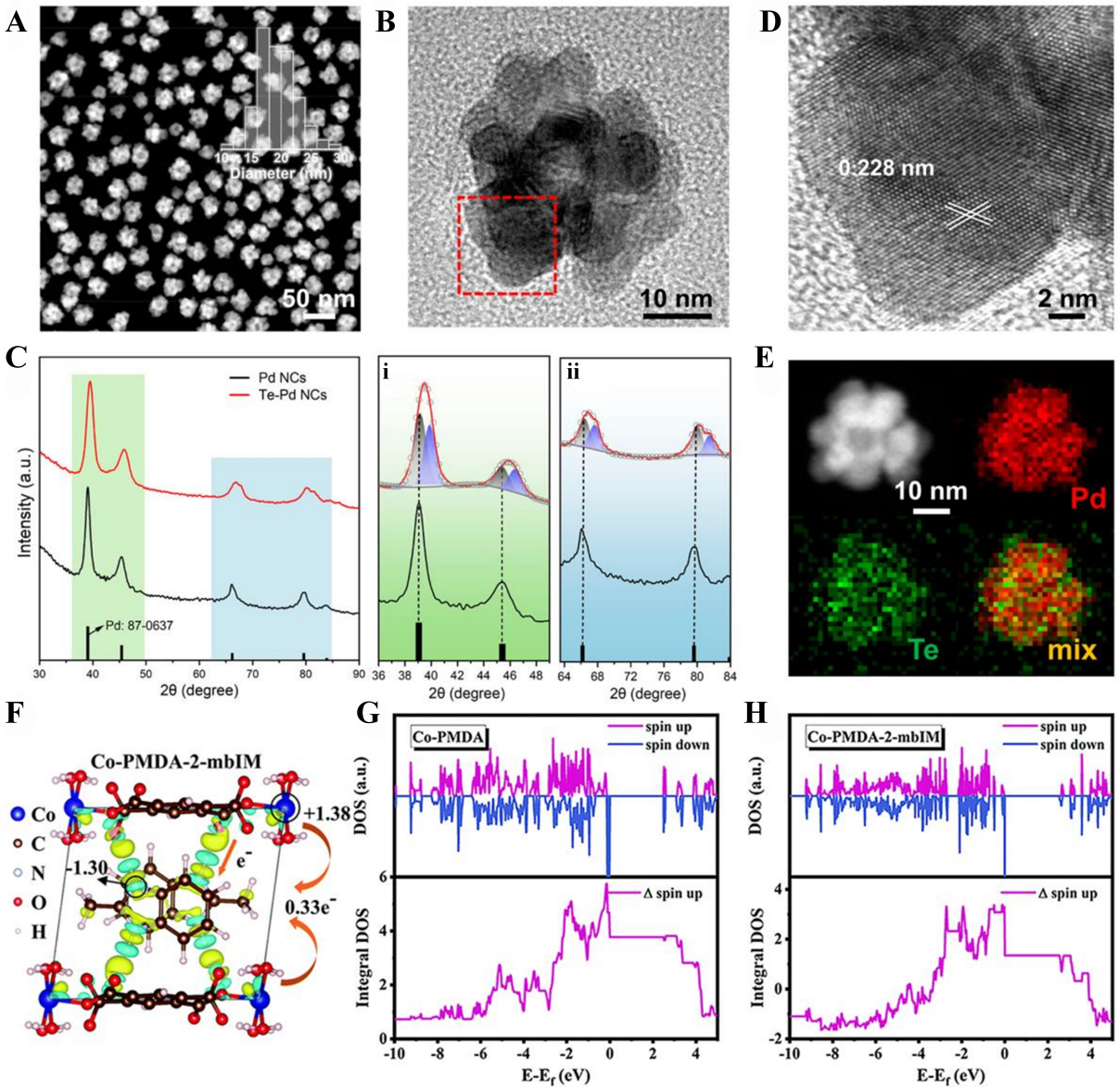

Figure 14. (A) HAADF-STEM with diameter histogram and (B) high-magnification TEM for Te-Pd NCs; (C) PXRD for Pd NCs and Te-Pd NCs. (i and ii) PXRD patterns enlarged from (C); (D) HRTEM for Te-Pd NCs from eectangular region in (B); (E) HAADF-STEM as well as elemental mappings of Te-Pd NCs. Reprinted with permission from ref[22]. Copyright 2020 American Chemical Society; (F) The charge density difference and the corresponding results for Bader charge analysis of Co-PMDA-2-mbIM; the yellow indicates electron accumulation and the cyan indicates electron depletion, the isosurface value is 0.0025 e·Bohr^{-3}; (G and H) The DOS and integral DOS for (G) Co-PMDA and (H) Co-PMDA-2-mbIM. Reprinted with permission from ref[50]. Copyright 2022 The Royal Society of Chemistry. HAADF-STEM: High-angle annular dark-field-scanning transmission electron microscopy; TEM: transmission electron microscopy; NCs: nanocrystals; PXRD: powder X-ray diffraction; HRTEM: high-resolution transmission electron microscope; PMDA: pyrodimethyl dianhydride; 2-mbIM: 2-methylbenzimidazole; DOS: density of states.

Doping heteroatoms on metal substrate

Doping heteroatoms are an effective strategy for improving the adsorption energy of intermediates by adjusting the surface electron structure[87,88]. Feng *et al.* reported a Te-doped Pd NC catalyst to synthesize urea through coupling CO_2RR with nitrite reduction [Figure 14A-E][22]. The doping of Te promoted not only the adsorption of CO_2 to form $^*CO$ but also the production of NH_3, satisfying the needs of urea formation. Under the optimized flow cell, the urea concentration reached 0.95 wt%, and the N atom efficiency (NE) was 82.3%.

Metal-inorganic compound

In the DFT study of Zhu *et al.*, Mo_2B_2, Ti_2B_2, and Cr_2B_2, these types of 2D metal borides (MBenes), had strong intrinsic activity for urea formation and could simultaneously electrocatalyze N_2 and CO_2 coupling to urea under mild conditions[89]. Moreover, these MBenes could significantly inhibit the competitive reaction that reduced N_2 to NH_3. Qiu *et al.* synthesized a $CuSiO_x$ nanotube catalyst by a hydrothermal method using SiO_2 nanospheres as templates[90]. The article reports comparative experiments of $CuSiO_x$ with $CuGeO_3$ and $CuSnO_3$. The experimental results showed that the Cu-O-Si interface of $CuSiO_x$ displayed stronger hydrophilicity that facilitated the movement of NO_3^- within the nano-channels to arrive at the catalytic site. The EIS revealed that the Cu-O-Si interface had a lower charge transfer resistance which indicated a faster charge transference. What is more, $CuSiO_x$ had the largest ECSA, providing more active sites for the catalysis. It is worth noting that this study pioneered the use of pulsed electrolysis in the electrocatalytic urea synthesis process. This method was capable of surmounting the electrostatic repulsion which hindered the mass transfer of NO_2^- to the catalyst surface during electrocatalytic coupling. Compared with constant potential electrolysis, the performance under pulsed electrolysis was significantly improved, with the urea FE increasing by ~39% (constant potential: 57%, pulsed: 79%, at -0.20 V *vs.* RHE) and yield of urea increasing by ~2.4-fold (656.4 $\mu g \cdot h^{-1} \cdot mg^{-1}_{cat.}$, pulsed: 1,606.1 $\mu g \cdot h^{-1} \cdot mg^{-1}_{cat.}$ at -0.60 V *vs.* RHE). The advantages of pulsed electrolysis technology were also verified on $CuGeO_3$ and $CuSnO_3$.

Conductive metal-organic framework

Yuan *et al.* designed a unique new conductive metal-organic framework (MOF) Co-PMDA-2-mbIM [Figure 14F-H][50]. Conductive MOF had accessible access and uniform distribution of active nodes, which made it easy for reactants to approach the active nodes[91]. This intercalated 2-methyl benzimidazole guest molecules had lone-pair electrons, which enabled the acceleration of interior charge transfer, significantly enhancing the adsorbing and activating of N_2/CO_2. Through an established unique charge-transfer bridge, $^*CO$ intermediates would directly couple with $^*N{=}N^*$ intermediates and produce the $^*NCON^*$ urea precursor, thus facilitating further urea production. At -0.50 V (*vs.* RHE), the urea yield reached a remarkable 14.47 $mmol \cdot h^{-1} \cdot g^{-1}$, and the urea FE was 48.97%.

SUMMARY AND OUTLOOK

Electrocatalytic synthesis of urea under environmental conditions, different from traditional industrial synthesis methods at high temperatures and pressures (150~250 bar and 150~210 °C), substantially reduces the energy consumption. It is of fabulous significance with respect to resource consumption and environment conservation. What is more, the electrochemical synthesis of urea goes beyond the traditional single reaction with NH_3 as the raw material and greatly expands the sources of nitrogen-containing reaction raw materials (such as NO_2^-, NO_3^-, N_2, NO). It provides a guideline for catalytic reduction of NO_2^-/NO_3^- containing pollutants or toxic gases such as NO to urea, which is an environmentally friendly strategy. However, compared with industrial production, there are still many shortcomings in current urea electrocatalytic synthesis, such as low urea yield, low FE, unclear reaction mechanism, and immature process, *etc.*[18]. These are the key factors that make urea electrocatalytic synthesis possible only in the laboratory rather than for commercial production.

Thus, the future development direction of urea electrochemical synthesis is prospected. (1) Optimizing catalyst design[92-98]. For the target of increasing the amount of active sites, improving the adsorption and activation for reactants, selecting the favorable reaction path, and so on, the high-efficiency catalysts should be designed from the selection of material composition or optimization of the structure. In addition, in the

Table 2. The half-reactions of CO_2RR in aqueous solutions for the different hydrocarbon products (pH = 7)[17]

Reaction	E^0 (V *vs.* SHE)
CO_2 (g) + e^- → $^*CO_2^-$	-1.90
CO_2 (g) + 2H^+ + 2e^- → HCOOH (l)	-0.55
CO_2 (g) + 2H^+ + 2e^- → CO (g) + H_2O (l)	-0.52
2CO_2 (g) + 2H^+ + 2e^- → $H_2C_2O_4$ (l)	-0.91
CO_2 (g) + 4H^+ + 2e^- → HCHO (l) + H_2O (l)	-0.48
CO_2 (g) + 6H^+ + 6e^- → CH_3OH (l) + H_2O (l)	-0.38
CO_2 (g) + 8H^+ + 8e^- → CH_4 (g) + 2H_2O (l)	-0.24
2CO_2 (g) + 12H^+ + 12e^- → C_2H_4 (g) + 4H_2O (l)	-0.38
2CO_2 (g) + 12H^+ + 12e^- → C_2H_5OH (l) + 3H_2O (l)	-0.35
2CO_2 (g) + 14H^+ + 14e^- → C_2H_6 (g) + 4H_2O (l)	-0.28
3CO_2 (g) + 18H^+ + 18e^- → C_3H_7OH (l) + 5H_2O (l)	-0.30
2H^+ + 2e^- → H_2 (g)	-0.42

CO_2RR: reduction reaction of CO_2; SHE: standard hydrogen electrode.

studies that have been reported so far, most of the proposed efficient catalysts are still in the stage of theoretical calculation or laboratory construction and are expected to be put into industrial production for further research; (2) Optimizing the experiment process[99-101]. The synergistic efficiency of CO_2RR and NRR is a critical factor in the electrochemical synthesis of urea. CO_2RR belongs to the gas-phase reaction; NRR belongs to the liquid-phase reaction, while the catalyst is a solid-phase system. Therefore, balancing the reaction between the three phases is necessary, which is useful to reduce the unnecessary competing reactions. As shown in Table 2, CO_2 has a variety of electrochemical reduction products in aqueous solutions. Some of them (such as CO, HCOOH/$HCOO^-$, *etc.*) are readily obtained through the generation and desorption of intermediates at an early stage, with the H_2 from HER acting as by-products in the electrosynthesis of urea. Furthermore, same as urea, the co-reduction of CO_2 and N sources provides the possibility for the synthesis of amide and amine, *etc.*, via C-N coupling [Figure 15]. In addition to designing the structure of the catalysts, modifying the environmental conditions of the reaction can be advantageous in modulating the reaction. It has been demonstrated that Cu catalysts showed easier adsorption of $^*H$ than $^*CO$ when pH = 7[102]. And the coverage of CO could influence the selectivity of CO_2RR at high overpotentials[103]. The catalytic synthesis efficiency of urea can be further improved by optimizing the catalytic system and choosing electrolytic liquids with better coordination with raw materials, such as highly gas-soluble ionic liquids, to reduce unnecessary side reactions[92,104-107]. Alternatively, a more efficient reactor, such as the flow cell, is used to replace the H-cell to increase the material transport efficiency and improve the current density[93]; (3) In-depth study of C-N coupling mechanism. The unclear mechanism of reactions presents the most critical problem, particularly concerning the activation of reactants, the formation of key intermediates, and the reaction pathway of the coupling step. These aspects remain highly controversial at present[105]. Advanced *in situ* characterization methods such as Raman spectra, SR-FTIR, and online DEMS are needed to assist the mechanism research; (4) Find new carbon sources to replace the CO_2. Actually, Xiong *et al.* have demonstrated the feasibility of electrocatalytic oxidative coupling of CO with NH_3 on platinum for the synthesis of urea[108]. The optimum selectivity of urea was about 70% and the rate of electrocatalytic C–N bond formation was up to 100 $mmol \cdot h^{-1} \cdot g^{-1}$. This reaction pathway not only broke the situation where the carbon source for electrocatalytic synthesis of urea was only derived from CO_2, but also provided an attractive strategy along the lines of oxidative coupling. Additionally, Shi *et al.* successfully synthesized urea via electrochemical coupling of HCOOH and NO over Ag-Cu Janus nanoparticle catalysts[109]. This work obtained excellent yield and FE of urea. However, the HCOOH was derived from CO_2 in an aqueous solution reduced by hydrated electrons produced by irradiated SO_3^{2-}[110-113]. The carbon

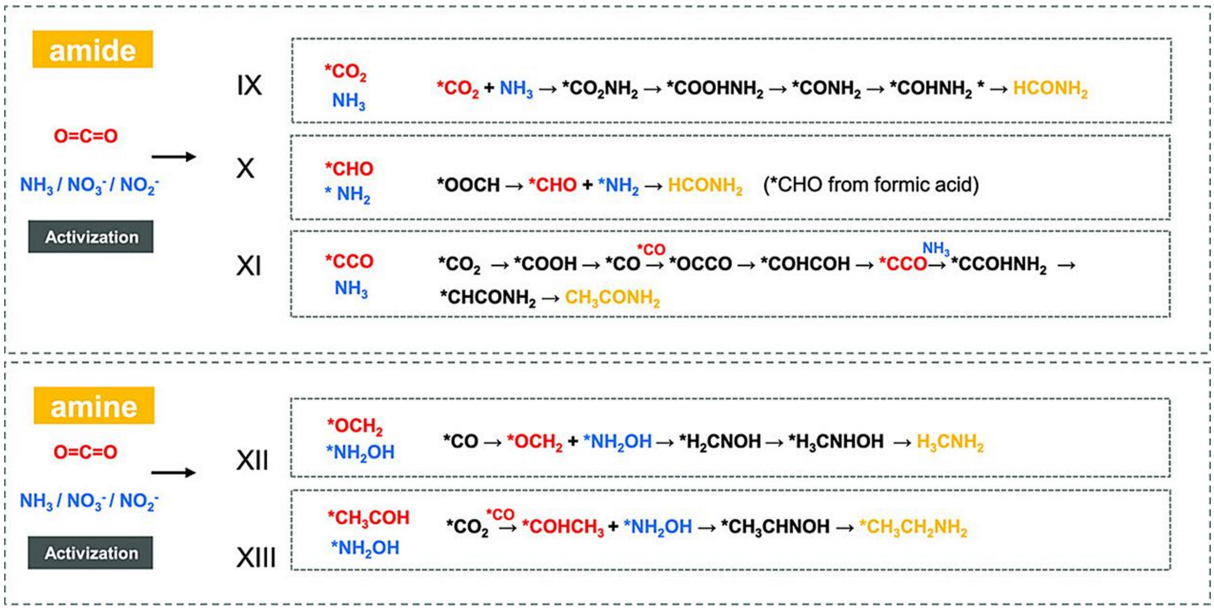

Figure 15. Mechanism of amide and amine from the co-reduction between CO_2 and NH_3/NO_3^-/NO_2^-. Reprinted with permission from ref[17]. Copyright 2023 The Authors. Advanced Energy and Sustainability Research published by Wiley-VCH GmbH.

source was still from CO_2 in essence. Therefore, the exploration of new carbon sources still has a long way to go.

DECLARATIONS

Authors' contributions

Writing-original draft: Cai H, Ding J, Liu W
Investigation: Hou T
Data curation, validation: Wei T, Liu Q, Luo J
Conceptualization, methodology, resources: Feng L, Liu X

Availability of data and materials

Not applicable.

Financial support and sponsorship

This work was financially supported by the Guangxi Natural Science Fund for Distinguished Young Scholars (2024GXNSFFA010008) , and the National Natural Science Foundation of China (22075211, 51971157, and 22275166).

Conflicts of interest

All authors declared that there are no conflicts of interest.

Ethical approval and consent to participate

Not applicable.

Consent for publication

Not applicable.

REFERENCES

1. Kuhl KP, Hatsukade T, Cave ER, Abram DN, Kibsgaard J, Jaramillo TF. Electrocatalytic conversion of carbon dioxide to methane and methanol on transition metal surfaces. *J Am Chem Soc* 2014;136:14107-13. DOI PubMed
2. Aresta M, Dibenedetto A, Angelini A. Catalysis for the valorization of exhaust carbon: from CO_2 to chemicals, materials, and fuels. Technological use of CO_2. *Chem Rev* 2014;114:1709-42. DOI PubMed
3. Wang R, Wang Z, Xiang X, Zhang R, Shi X, Sun X. MnO_2 nanoarrays: an efficient catalyst electrode for nitrite electroreduction toward sensing and NH_3 synthesis applications. *Chem Commun* 2018;54:10340-2. DOI PubMed
4. Xu Y, Ren K, Ren T, et al. Cooperativity of Cu and Pd active sites in CuPd aerogels enhances nitrate electroreduction to ammonia. *Chem Commun* 2021;57:7525-8. DOI PubMed
5. Franz RA, Applegath F. A new urea synthesis. I. The reaction of ammonia, carbon monoxide, and sulfur. *J Org Chem* 1961;26:3304-5. DOI
6. Lahalih SM, Ahmed N. Effect of new soil stabilizers on the compressive strength of dune sand. *Constr Build Mater* 1998;12:321-8. DOI
7. Huang HM, McDouall JJW, Procter DJ. Radical anions from urea-type carbonyls: radical cyclizations and cyclization cascades. *Angew Chem Int Ed Engl* 2018;57:4995-9. DOI PubMed
8. Barzagli F, Mani F, Peruzzini M. From greenhouse gas to feedstock: formation of ammonium carbamate from CO_2 and NH_3 in organic solvents and its catalytic conversion into urea under mild conditions. *Green Chem* 2011;13:1267-74. DOI
9. Pérez-fortes M, Bocin-dumitriu A, Tzimas E. CO_2 utilization pathways: techno-economic assessment and market opportunities. *Energy Procedia* 2014;63:7968-75. DOI
10. Giddey S, Badwal S, Kulkarni A. Review of electrochemical ammonia production technologies and materials. *Int J Hydrogen Energ* 2013;38:14576-94. DOI
11. Smil V. Detonator of the population explosion. *Nature* 1999;400:415. DOI
12. Bao D, Zhang Q, Meng FL, et al. Electrochemical reduction of N_2 under ambient conditions for artificial N_2 fixation and renewable energy storage using N_2/NH_3 cycle. *Adv Mater* 2017;29:1604799. DOI PubMed
13. Chen C, Zhu X, Wen X, et al. Coupling N_2 and CO_2 in H_2O to synthesize urea under ambient conditions. *Nat Chem* 2020;12:717-24. DOI PubMed
14. Fu J, Yang Y, Hu J. Dual-sites tandem catalysts for C–N bond formation via electrocatalytic coupling of CO_2 and nitrogenous small molecules. *ACS Mater Lett* 2021;3:1468-76. DOI
15. Planas N, Dzubak AL, Poloni R, et al. The mechanism of carbon dioxide adsorption in an alkylamine-functionalized metal-organic framework. *J Am Chem Soc* 2013;135:7402-5. DOI PubMed
16. Jouny M, Lv JJ, Cheng T, et al. Formation of carbon-nitrogen bonds in carbon monoxide electrolysis. *Nat Chem* 2019;11:846-51. DOI PubMed
17. Liu J, Zhang X, Yang R, Yang Y, Wang X. Electrocatalytic reduction of CO_2 to value-added chemicals via C–C/N coupling. *Adv Energ Sust Res* 2023;4:2200192. DOI
18. Jiang M, Zhu M, Wang M, et al. Review on electrocatalytic coreduction of carbon dioxide and nitrogenous species for urea synthesis. *ACS Nano* 2023;17:3209-24. DOI PubMed
19. Chen C, He N, Wang S. Electrocatalytic C–N coupling for urea synthesis. *Small Sci* 2021;1:2100070. DOI
20. Shibata M, Yoshida K, Furuya N. Electrochemical synthesis of urea on reduction of carbon dioxide with nitrate and nitrite ions using Cu-loaded gas-diffusion electrode. *J Electroanal Chem* 1995;387:143-5. DOI
21. Cao N, Quan Y, Guan A, et al. Oxygen vacancies enhanced cooperative electrocatalytic reduction of carbon dioxide and nitrite ions to urea. *J Colloid Interface Sci* 2020;577:109-14. DOI PubMed
22. Feng Y, Yang H, Zhang Y, et al. Te-doped Pd nanocrystal for electrochemical urea production by efficiently coupling carbon dioxide reduction with nitrite reduction. *Nano Lett* 2020;20:8282-9. DOI PubMed
23. Meng N, Huang Y, Liu Y, Yu Y, Zhang B. Electrosynthesis of urea from nitrite and CO_2 over oxygen vacancy-rich ZnO porous nanosheets. *Cell Rep Phys Sci* 2021;2:100378. DOI
24. Zhang C, Shi Y, Yu Y, Du Y, Zhang B. Engineering sulfur defects, atomic thickness, and porous structures into cobalt sulfide nanosheets for efficient electrocatalytic alkaline hydrogen evolution. *ACS Catal* 2018;8:8077-83. DOI
25. Jia R, Wang Y, Wang C, Ling Y, Yu Y, Zhang B. Boosting selective nitrate electroreduction to ammonium by constructing oxygen vacancies in TiO_2. *ACS Catal* 2020;10:3533-40. DOI
26. Zhang J, Yin R, Shao Q, Zhu T, Huang X. Oxygen vacancies in amorphous InO_x nanoribbons enhance CO_2 adsorption and activation for CO_2 electroreduction. *Angew Chem Int Ed Engl* 2019;58:5609-13. DOI PubMed
27. Huang Y, Yang R, Wang C, et al. Direct electrosynthesis of urea from carbon dioxide and nitric oxide. *ACS Energy Lett* 2022;7:284-91. DOI
28. Long J, Chen S, Zhang Y, et al. Direct electrochemical ammonia synthesis from nitric oxide. *Angew Chem Int Ed Engl* 2020;59:9711-8. DOI PubMed

29. Lv C, Zhong L, Liu H, et al. Selective electrocatalytic synthesis of urea with nitrate and carbon dioxide. *Nat Sustain* 2021;4:868-76. DOI
30. Lv C, Lee C, Zhong L, et al. A defect engineered electrocatalyst that promotes high-efficiency urea synthesis under ambient conditions. *ACS Nano* 2022;16:8213-22. DOI PubMed
31. Luo Y, Xie K, Ou P, et al. Selective electrochemical synthesis of urea from nitrate and CO_2 via relay catalysis on hybrid catalysts. *Nat Catal* 2023;6:939-48. DOI
32. Meng N, Ma X, Wang C, et al. Oxide-derived core-shell Cu@Zn nanowires for urea electrosynthesis from carbon dioxide and nitrate in water. *ACS Nano* 2022;16:9095-104. DOI PubMed
33. Leverett J, Tran-Phu T, Yuwono JA, et al. Tuning the coordination structure of Cu–N–C single atom catalysts for simultaneous electrochemical reduction of CO_2 and NO_3^- to urea. *Adv Energy Mater* 2022;12:2201500. DOI
34. Zhang X, Zhu X, Bo S, et al. Identifying and tailoring C-N coupling site for efficient urea synthesis over diatomic Fe-Ni catalyst. *Nat Commun* 2022;13:5337. DOI PubMed PMC
35. Wei X, Liu Y, Zhu X, et al. Dynamic reconstitution between copper single atoms and clusters for electrocatalytic urea synthesis. *Adv Mater* 2023;35:e2300020. DOI PubMed
36. Yuan M, Chen J, Xu Y, et al. Highly selective electroreduction of N_2 and CO_2 to urea over artificial frustrated Lewis pairs. *Energy Environ Sci* 2021;14:6605-15. DOI
37. Melen RL. A step closer to metal-free dinitrogen activation: a new chapter in the chemistry of frustrated Lewis pairs. *Angew Chem Int Ed Engl* 2018;57:880-2. DOI PubMed
38. Zhang L, Liang J, Wang Y, et al. High-performance electrochemical NO reduction into NH_3 by MoS_2 nanosheet. *Angew Chem Int Ed Engl* 2021;60:25263-8. DOI PubMed
39. Yuan M, Chen J, Bai Y, et al. Unveiling electrochemical urea synthesis by co-activation of CO_2 and N_2 with Mott-Schottky heterostructure catalysts. *Angew Chem Int Ed Engl* 2021;60:10910-8. DOI PubMed
40. He K, Tadesse Tsega T, Liu X, et al. Utilizing the space-charge region of the FeNi-LDH/CoP p-n junction to promote performance in oxygen evolution electrocatalysis. *Angew Chem Int Ed Engl* 2019;58:11903-9. DOI PubMed
41. Bo Y, Wang H, Lin Y, et al. Altering hydrogenation pathways in photocatalytic nitrogen fixation by tuning local electronic structure of oxygen vacancy with dopant. *Angew Chem Int Ed Engl* 2021;60:16085-92. DOI PubMed
42. Liu S, Yin S, Wang Z, et al. AuCu nanofibers for electrosynthesis of urea from carbon dioxide and nitrite. *Cell Rep Phys Sci* 2022;3:100869. DOI
43. Huang Y, Wang Y, Liu Y, et al. Unveiling the quantification minefield in electrocatalytic urea synthesis. *Chem Eng J* 2023;453:139836. DOI
44. Zhao Y, Ding Y, Li W, et al. Efficient urea electrosynthesis from carbon dioxide and nitrate via alternating Cu-W bimetallic C-N coupling sites. *Nat Commun* 2023;14:4491. DOI PubMed PMC
45. Lv L, Tan H, Kong Y, et al. Breaking the scaling relationship in C-N coupling via the doping effects for efficient urea electrosynthesis. *Angew Chem Int Ed Engl* 2024;63:e202401943. DOI PubMed
46. Saravanakumar D, Song J, Lee S, Hur NH, Shin W. Electrocatalytic conversion of carbon dioxide and nitrate ions to urea by a Titania-Nafion composite electrode. *ChemSusChem* 2017;10:3999-4003. DOI PubMed
47. Geng J, Ji S, Jin M, et al. Ambient electrosynthesis of urea with nitrate and carbon dioxide over iron-based dual-sites. *Angew Chem Int Ed Engl* 2023;62:e202210958. DOI PubMed PMC
48. Hou T, Ding J, Zhang H, et al. $FeNi_3$ nanoparticles for electrocatalytic synthesis of urea from carbon dioxide and nitrate. *Mater Chem Front* 2023;7:4952-60. DOI
49. Yu X, Zeng S, Li L, Yao H, Zheng Y, Guo X. Synergistic coupling of CO_2 and NO_3^- for efficient electrosynthesis of urea using oxygen vacancy-rich Ru-doped CeO_2 nanorods. *Sci China Mater* 2024;67:1543-50. DOI
50. Yuan M, Chen J, Zhang H, et al. Host–guest molecular interaction promoted urea electrosynthesis over a precisely designed conductive metal–organic framework. *Energy Environ Sci* 2022;15:2084-95. DOI
51. Chen X, Lv S, Kang J, et al. Efficient C-N coupling in the direct synthesis of urea from CO_2 and N_2 by amorphous $Sb_xBi_{1-x}O_y$ clusters. *Proc Natl Acad Sci U S A* 2023;120:e2306841120. DOI PubMed PMC
52. Govindan B, Annamalai K, Kumar A, Palanisamy S, Abu Haija M, Banat F. Synergistic bimetallic sites in 2D-on-2D heterostructures for enhanced C–N coupling in sustainable urea synthesis. *ACS Sustain Chem Eng* 2024;12:8174-87. DOI
53. Jeon HS, Sinev I, Scholten F, et al. Operando evolution of the structure and oxidation state of size-controlled Zn nanoparticles during CO_2 electroreduction. *J Am Chem Soc* 2018;140:9383-6. DOI PubMed
54. Zhao X, Zhao H, Sun J, Li G, Liu R. Blocking the defect sites on ultrathin Pt nanowires with Rh atoms to optimize the reaction path toward alcohol fuel oxidation. *Chinese Chem Lett* 2020;31:1782-6. DOI
55. Chang F, Shan S, Petkov V, et al. Composition tunability and (111)-dominant facets of ultrathin platinum-gold alloy nanowires toward enhanced electrocatalysis. *J Am Chem Soc* 2016;138:12166-75. DOI PubMed
56. Kim D, Xie C, Becknell N, et al. Electrochemical activation of CO_2 through atomic ordering transformations of AuCu nanoparticles. *J Am Chem Soc* 2017;139:8329-36. DOI PubMed
57. Yu Y, Wang C, Yu Y, Wang Y, Zhang B. Promoting selective electroreduction of nitrates to ammonia over electron-deficient Co modulated by rectifying Schottky contacts. *Sci China Chem* 2020;63:1469-76. DOI
58. Won DH, Shin H, Koh J, et al. Highly efficient, selective, and stable CO_2 electroreduction on a hexagonal Zn catalyst. *Angew Chem*

Int Ed Engl 2016;55:9297-300. DOI PubMed

59. Lu L, Sun X, Ma J, et al. Highly efficient electroreduction of CO_2 to methanol on palladium-copper bimetallic aerogels. *Angew Chem Int Ed Engl* 2018;57:14149-53. DOI PubMed
60. Siva P, Prabu P, Selvam M, Karthik S, Rajendran V. Electrocatalytic conversion of carbon dioxide to urea on nano-$FeTiO_3$ surface. *Ionics* 2017;23:1871-8. DOI
61. Yang M, Wei T, He J, et al. Au nanoclusters anchored on TiO_2 nanosheets for high-efficiency electroreduction of nitrate to ammonia. *Nano Res* 2024;17:1209-16. DOI
62. Ma S, Lan Y, Perez GM, Moniri S, Kenis PJ. Silver supported on titania as an active catalyst for electrochemical carbon dioxide reduction. *ChemSusChem* 2014;7:866-74. DOI PubMed
63. Wang H, Zhang F, Jin M, et al. V-doped TiO_2 nanobelt array for high-efficiency electrocatalytic nitrite reduction to ammonia. *Mater Today Phys* 2023;30:100944. DOI
64. Zhao Y, Zhao Y, Shi R, et al. Tuning oxygen vacancies in ultrathin TiO_2 nanosheets to boost photocatalytic nitrogen fixation up to 700 nm. *Adv Mater* 2019;31:e1806482. DOI PubMed
65. Cao N, Chen Z, Zang K, et al. Doping strain induced bi-Ti^{3+} pairs for efficient N_2 activation and electrocatalytic fixation. *Nat Commun* 2019;10:2877. DOI PubMed PMC
66. Han Z, Choi C, Hong S, et al. Activated TiO_2 with tuned vacancy for efficient electrochemical nitrogen reduction. *Appl Catal B Environ* 2019;257:117896. DOI
67. Stephan DW. Frustrated Lewis Pairs. *J Am Chem Soc* 2015;137:10018-32. DOI PubMed
68. Dong Y, Ghuman KK, Popescu R, et al. Tailoring surface frustrated Lewis pairs of $In_2O_{3-x}(OH)_y$ for gas-phase heterogeneous photocatalytic reduction of CO_2 by isomorphous substitution of In^{3+} with Bi^3. *Adv Sci* 2018;5:1700732. DOI PubMed PMC
69. Shan W, Liu R, Zhao H, et al. *In Situ* surface-enhanced raman spectroscopic evidence on the origin of selectivity in CO_2 electrocatalytic reduction. *ACS Nano* 2020;14:11363-72. DOI PubMed
70. He Y, He Q, Wang L, et al. Self-gating in semiconductor electrocatalysis. *Nat Mater* 2019;18:1098-104. DOI PubMed
71. Xu L, Wang C, Zhang X, et al. NO_x sensitivity of conductometric $In(OH)_3$ sensors operated at room temperature and transition from p- to n- type conduction. *Sensor Actuat B Chem* 2017;245:533-40. DOI
72. Gavali DS, Kawazoe Y, Thapa R. First-principles identification of interface effect on Li storage capacity of C_3N/graphene multilayer heterostructure. *J Colloid Interface Sci* 2022;610:80-8. DOI PubMed
73. Roy P, Pramanik A, Sarkar P. Dual-silicon-doped graphitic carbon nitride sheet: an efficient metal-free electrocatalyst for urea synthesis. *J Phys Chem Lett* 2021;12:10837-44. DOI PubMed
74. Dutta S, Pati SK. Urea production on metal-free dual silicon doped C_9N_4 nanosheet under ambient conditions by electrocatalysis: a first principles study. *Chemphyschem* 2023;24:e202200453. DOI PubMed
75. Liu S, Jin M, Sun J, et al. Coordination environment engineering to boost electrocatalytic CO_2 reduction performance by introducing boron into single-Fe-atomic catalyst. *Chem Eng J* 2022;437:135294. DOI
76. Wu H, Fei G, Gao X, et al. Research progress on preparation and application of polyaniline and its composite materials. *China Powder Sci Technol* 2023;29:70-80. DOI
77. Jiao L, Zhu J, Zhang Y, et al. Non-bonding interaction of neighboring Fe and Ni single-atom pairs on MOF-derived N-doped carbon for enhanced CO_2 electroreduction. *J Am Chem Soc* 2021;143:19417-24. DOI PubMed
78. Chen K, Cao M, Ni G, et al. Nickel polyphthalocyanine with electronic localization at the nickel site for enhanced CO_2 reduction reaction. *Appl Catal B Environ* 2022;306:121093. DOI
79. Zhang H, Wang C, Luo H, Chen J, Kuang M, Yang J. Iron nanoparticles protected by chainmail-structured graphene for durable electrocatalytic nitrate reduction to nitrogen. *Angew Chem Int Ed Engl* 2023;62:e202217071. DOI PubMed
80. Zhu C, Geng Y, Yao X, Zhu G, Su Z, Zhang M. Fascinating electrocatalysts with dispersed di-metals in MN_3-M'N_4 moiety as two active sites separately for N_2 and CO_2 reduction reactions and jointly for C–N coupling and urea production. *Small Methods* 2023;7:e2201331. DOI PubMed
81. Shi MM, Bao D, Wulan BR, et al. Au sub-nanoclusters on TiO_2 toward highly efficient and selective electrocatalyst for N_2 conversion to NH_3 at ambient conditions. *Adv Mater* 2017;29:1606550. DOI PubMed
82. Shi M, Bao D, Li S, Wulan B, Yan J, Jiang Q. Anchoring PdCu amorphous nanocluster on graphene for electrochemical reduction of N_2 to NH_3 under ambient conditions in aqueous solution. *Adv Energy Mater* 2018;8:1800124. DOI
83. Qiao B, Wang A, Yang X, et al. Single-atom catalysis of CO oxidation using Pt1/FeO_x. *Nat Chem* 2011;3:634-41. DOI PubMed
84. Shibata M, Furuya N. Electrochemical synthesis of urea at gas-diffusion electrodes: Part VI. Simultaneous reduction of carbon dioxide and nitrite ions with various metallophthalocyanine catalysts. *J Electroanal Chem* 2001;507:177-84. DOI
85. Yang JP, Zhang FZ, Chen J. Structural design and application of fiber-based electrocatalytic materials. *China Powder Sci Technol* 2024;30:161-70. DOI
86. Kayan DB, Köleli F. Simultaneous electrocatalytic reduction of dinitrogen and carbon dioxide on conducting polymer electrodes. *Appl Catal B Environ* 2016;181:88-93. DOI
87. Tao H, Sun X, Back S, et al. Doping palladium with tellurium for the highly selective electrocatalytic reduction of aqueous CO_2 to CO. *Chem Sci* 2018;9:483-7. DOI PubMed PMC
88. Zhang Q, Wang K, Zhang M, et al. Electronic structure optimization boosts Pd nanocrystals for ethanol electrooxidation realized by Te doping. *CrystEngComm* 2022;24:5580-7. DOI
89. Zhu X, Zhou X, Jing Y, Li Y. Electrochemical synthesis of urea on MBenes. *Nat Commun* 2021;12:4080. DOI PubMed PMC

90. Qiu W, Qin S, Li Y, et al. Overcoming electrostatic interaction via pulsed electroreduction for boosting the electrocatalytic urea synthesis. *Angew Chem Int Ed Engl* 2024;63:e202402684. DOI PubMed
91. Wang XL, Dong LZ, Qiao M, et al. Exploring the performance improvement of the oxygen evolution reaction in a stable bimetal-organic framework system. *Angew Chem Int Ed Engl* 2018;57:9660-4. DOI PubMed
92. König M, Vaes J, Klemm E, Pant D. Solvents and supporting electrolytes in the electrocatalytic reduction of CO_2. *iScience* 2019;19:135-60. DOI PubMed PMC
93. Ren S, Joulié D, Salvatore D, et al. Molecular electrocatalysts can mediate fast, selective CO_2 reduction in a flow cell. *Science* 2019;365:367-9. DOI PubMed
94. Chen S, Lian K, Liu W, et al. Engineering active sites of cathodic materials for high-performance Zn-nitrogen batteries. *Nano Res* 2023;16:9214-30. DOI
95. Wang L, Wu J, Wang S, Liu H, Wang Y, Wang D. The reformation of catalyst: from a trial-and-error synthesis to rational design. *Nano Res* 2024;17:3261-301. DOI
96. Li R, Wang D. Understanding the structure-performance relationship of active sites at atomic scale. *Nano Res* 2022;15:6888-923. DOI
97. Qi D, Lv F, Wei T, et al. High-efficiency electrocatalytic NO reduction to NH_3 by nanoporous VN. *Nano Res Energy* 2022;1:e9120022. DOI
98. Liu W, Niu X, Tang J, et al. Energy-efficient anodic reactions for sustainable hydrogen production via water electrolysis. *Chem Synth* 2023;3:44. DOI
99. Chen C, Li S, Zhu X, et al. Balancing sub-reaction activity to boost electrocatalytic urea synthesis using a metal-free electrocatalyst. *Carbon Energy* 2023;5:e345. DOI
100. Wang X, Zhang G, Yin W, et al. Metal–organic framework-derived phosphide nanomaterials for electrochemical applications. *Carbon Energy* 2022;4:246-81. DOI
101. Zheng X, Li B, Wang Q, Wang D, Li Y. Emerging low-nuclearity supported metal catalysts with atomic level precision for efficient heterogeneous catalysis. *Nano Res* 2022;15:7806-39. DOI
102. Liu X, Chen M, Ma J, et al. Advances in the synthesis strategies of carbon□based single-atom catalysts and their electrochemical applications. *China Powder Sci Technol* 2024;30:35-45. DOI
103. Liu X, Schlexer P, Xiao J, et al. pH effects on the electrochemical reduction of $CO_{(2)}$ towards C_2 products on stepped copper. *Nat Commun* 2019;10:32. DOI PubMed PMC
104. Yang Y, Zhang W, Chen K, et al. Research progress on adsorption mechanism of radioactive iodine by metal-organic framework composites. *China Powder Sci Technol* 2024;30:151-60. DOI
105. Fan Q, Su J, Sun T, et al. Advances of the functionalized carbon nitrides for electrocatalysis. *Carbon Energy* 2022;4:211-36. DOI
106. Gan T, Wang D. Atomically dispersed materials: ideal catalysts in atomic era. *Nano Res* 2024;17:18-38. DOI
107. Cao N, Zhang N, Wang K, Yan K, Xie P. High-throughput screening of B/N-doped graphene supported single-atom catalysts for nitrogen reduction reaction. *Chem Synth* 2023;3:23. DOI
108. Xiong H, Yu P, Chen K, et al. Urea synthesis via electrocatalytic oxidative coupling of CO with NH_3 on Pt. *Nat Catal* 2024;7:785-95. DOI
109. Shi Z, Chen J, Li K, Liu Y, Tang Y, Zhang L. Flue gas to urea: a path of flue gas resourceful utilization through electrocatalysis. *Chem Eng J* 2023;461:141933. DOI
110. Ding S, Wang H, Dai X, et al. Mn-modulated Co–N–C oxygen electrocatalysts for robust and temperature-adaptative zinc-air batteries. *Chinese J Struc Chem* 2024;43:100302. DOI
111. Ji Y, Yu Z, Yan L, Song W. Research progress in preparation, modification and application of biomass-based single-atom catalysts. *China Powder Sci Technol* 2023;29:100-7. DOI
112. Zhang C, Xu H, Wang Y, et al. Reduction of 4-nitrophenol with nano-gold@graphene composite porous material. *China Powder Sci Technol* 2023;29:80-93. DOI
113. Wang H, Niu X, Liu W, et al. S-block metal Mg-mediated Co–N–C as efficient oxygen electrocatalyst for durable and temperature-adapted Zn-air batteries. *Adv Sci* 2024:e2403865. DOI PubMed